Data Driven Model Order Reduction of Gas Distribution Network

By

Muhammad Altaf Khattak

Spring 2019-MS-CS&E 00000281789

Supervisor

Dr. Mian Ilyas Ahmad

Department of Computational Science and Engineering

Research Centre for Modelling and Simulation

National University of Sciences and Technology (NUST)

Islamabad, Pakistan

October 2021

Data Driven Model Order Reduction of Gas Distribution Network

By

Muhammad Altaf Khattak

Spring 2019-MS-CS&E 00000281789

Supervisor

Dr. Mian Ilyas Ahmad

A thesis submitted in conformity with the requirements for the degree of *Master of Science* in Computational Science and Engineering

Research Centre for Modelling and Simulation,
National University of Sciences and Technology (NUST)
Islamabad, Pakistan

October 2021

Declaration

I, *Muhammad Altaf Khattak* declare that this thesis titled "Data Driven Model Order Reduction of Gas Distribution Network" and the work presented in it are my own and has been generated by me as a result of my own original research.

I confirm that:

1. This work was done wholly or mainly while in candidature for a Master of Science degree at NUST
2. Where any part of this thesis has previously been submitted for a degree or any other qualification at NUST or any other institution, this has been clearly stated
3. Where I have consulted the published work of others, this is always clearly attributed
4. Where I have quoted from the work of others, the source is always given. With the exception of such quotations, this thesis is entirely my own work
5. I have acknowledged all main sources of help
6. Where the thesis is based on work done by myself jointly with others, I have made clear exactly what was done by others and what I have contributed myself

---

Muhammad Altaf Khattak,
MS-CS&E-RCMS 00000281789

Copyright Notice

This thesis is dedicated to *my beloved parents and my sister*

Acknowledgments

I am thankful to my Creator Allah Subhana-Watala to have guided me throughout this work at every step and for every new thought which You setup in my mind to improve it. Indeed I could have done nothing without Your priceless help and guidance. Whosoever helped me throughout the course of my thesis, whether my parents or any other individual was Your will, so indeed none be worthy of praise but You.

I am profusely thankful to my beloved parents who raised me when I was not capable of walking and continued to support me throughout in every department of my life.

I would also like to express special thanks to my supervisor Dr. Mian Ilyas Ahmad for his help throughout my thesis and also for the courses which he has taught me. I can safely say that I haven't learned any other engineering subject in such depth than the ones which he has taught.

I would also like to thank Dr. Zartasha Mustansar, Dr. Absaar Ul Jabbar and Dr. Israr Ud Din for being on my thesis guidance and evaluation committee.

Finally, I would like to express my gratitude to all the individuals who have rendered valuable assistance to my study.

Contents

List of Figures

List of Tables

List of Abbreviations and Symbols

Abbreviations

MOR	Model Order Reduction
ROM	Reduced Order Model
PDE	Partial Differential Equation
ODE	Ordinary Differential Equation
DAE	Differential Algebraic Equation
FVM	Finite Volume Method
FDM	Finite Difference Method
FOM	Full Order Model
LTI	Linear Time Invariant
DP	Dynamic Programming
ROM	Reduced Order Model
SECM	Scanning Electrochemical Microscope
VLSI	Very Large Scale Integration
PMOR	Parametric Model Order Reduction
DP	Dynamic Programming

CFD	Computational Fluid Dynamics
SVD	Singular Value Decomposition
POD	Proper Orthogonal Decomposition
QB	Quadratic Bilinear System
QBDAE	Quadratic Bilinear Differential Algebraic Equations

Abstract

Natural gas is distributed through a complex network of pipes, nodes (supply and demand), compressors and control valves covering a large geographical area. To observe the behaviour of such complex network, typical procedure is to use multiple measurement devices at different nodes/regions and record the flow and pressure of gas at those points. This procedure is complex, time consuming, requires large number of human resources and involves human/ measurement device errors. An alternate is to use mathematical modelling and simulation of gas distribution network where the mathematical model involves differential as well as algebraic equations that lead to the so-called descriptor system. It is known in the literature that simulation of such complex systems is computationally expensive. To resolve this issue, the concept of model order reduction can be used in which a reduced order model is constructed from the original large scale model such that the behaviour is approximately same. In this thesis we used a specific model order reduction technique that is the Loewner framework which is data driven and interpolating the original system. The Loewner framework constructs reduced order model without relying on the use of original model; instead, it uses pair of datasets at given interpolation points. The approach provides trade-off between the accuracy of fit and size of reduced order model. In this thesis, the applicability of Loewner framework for reduction of gas distribution network has been tested and implemented on some numerical examples. The expansion to nonlinear (quadratic-bilinear) model of gas distribution network is also considered using nonlinear projection based interpolatory model order reduction techniques. Numerical results show that reduced order model is highly accurate, stable and takes lesser time to simulate as compared to the original model.

Keywords: *Gas distribution network, partial differential equation, data driven model order reduction*

Chapter 1

Introduction

This chapter starts with introduction of modelling and simulation of gas distribution network. The advantage of using model order reduction (MOR) in the field of modelling and simulation is also discussed. The problem statement is discussed afterwards. The application of MOR in simulation of gas distribution network is also discussed. In the end of this chapter, thesis overview is given.

1.1 Gas Distribution Network

In the coming decades, natural gas will be one of the most important energy sources. The known natural gas deposits, using new techniques, such as hydraulic fracturing, have the potential for at least another century to fuel our world. Natural gas is easy to transport and store, it is widely used to generate electricity and heat. Pakistan accounts for about 1.2 percent of world natural gas output while also having the greatest percentage of domestic energy production at 88.69 percent, with the remaining 11.31 percent consisting of nuclear, hydropower, fossil fuels, and renewable energy [1]. The high-pressure transport network and the low-pressure distribution network are used to transport natural gas directly from the source refinery via a network of numerous pipelines. The transportation of natural gas through pipes help us store extra gas in the storage tanks. Pipeline systems are widely used for the transmission of gas, oil, water, and chemicals because they are more resource-efficient than other means of transportation [2]. pipeline systems can categorised as: high pressure transmission system and low pressure distribution system. Transmission network usually comprises of

pipes with longer lengths and bigger diameters as compared to low pressure distribution network. The entire transportation network of natural gas is made up of integrated system of low pressure and high pressure pipes that can be grouped as: upstream, midstream and downstream. Hydraulic fracturing, horizontal drilling, and acidizing are all used in the upstream sector to extract gas from gas and oil reservoirs. The raw gas is delivered to gas refineries via small-diameter, low-pressure collecting pipelines because it is not fit for consumption. The midstream sector serves as a key connection between manufacturing facilities and demand centres which consists of gas gathering and processing plants. It is also responsible for flow of gas in high pressure pipes. The downstream industries include distribution companies which provide natural gas to consumers through certain distribution network. The block diagram in Figure 1.1.

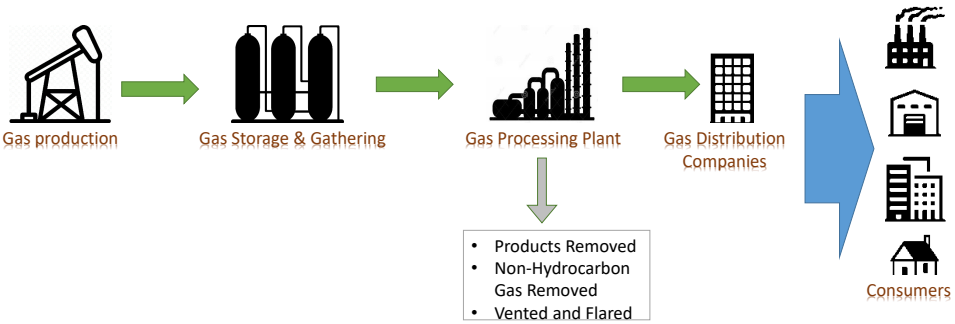

Figure 1.1: Structure of Gas Transportation Network

The components of gas transportation network are:

- Pipes: Gas network consists of high pressure pipes which are used for flow of gas over the long distances while low pressure pipes are used for shorter distances.
- Compressors: To ensure the flow of gas with certain pressure, compressors are used in the pipeline structure of gas network.
- Nodes: It can be supply node through which gas enters into the network, demand node where gas is taken from the network and junction node which are used to connect two or more pipes.

- Control Valves: To control the flow of gas in the network, control valves are used in the gas network.
- Storage Tank: To meet the sudden growing demand of the gas in a network, storage tanks are used to ensure the constant flow of gas.

1.2 MOR and its Mathematical Formulation

Most physical phenomena get the shape of the partial differential equations (PDEs) when modelled. Only simple geometries have an analytical solution for describing PDEs for each component. But it is possible to evaluate either approximation or numerical solution of the system when there are complex geometries. Numerical solution assists in the study of complex physical underlying systems. More detail in the output is required for precision. To find comprehensive detail in the output, many possible realizations must be simulated, resulting in a more complex large-scale model. High computational power is required to simulate such large-scale models.

Originally, MOR was worked out in system analysis and control theory, which focuses on the properties of dynamic systems in application to reduce their complex structure while maintaining as much of their input-output behaviour as possible. To understand the concept of MOR, let us consider a system which can be written in the form of nonlinear state space model explained in [3]:

$$\begin{aligned} \dot{x}(t) &= f(x(t), u(t)), \\ y(t) &= h(x(t), u(t)), \end{aligned} \tag{1.2.1}$$

where f, h are nonlinear functions i.e. f, h : $\mathbb{R}^n \to \mathbb{R}^n$, $u(t) \in \mathbb{R}^m$ represents input of the model, $x(t) \in \mathbb{R}^n$ represents the states of the original model and $y(t) \in \mathbb{R}^p$ is output of the model.

Now using MOR technique, an approximation of the model in (1.2.1) is required which can be represented as:

$$\begin{aligned} \hat{\dot{x}}(t) &= \hat{f}(\hat{x}(t), u(t)), \\ \hat{y}(t) &= \hat{h}(\hat{x}(t), u(t)), \end{aligned} \tag{1.2.2}$$

where $\hat{f}$ and $\hat{h}$ are nonlinear functions i.e.$\hat{f}, \hat{h} : \mathbb{R}^r \to \mathbb{R}^r$, $\hat{x}(t) \in \mathbb{R}^r$ denotes the state and $\hat{y}(t) \in \mathbb{R}^p$ represents output of the approximated model given in (1.2.2). This model is known as reduced order model (ROM) and can be used for simulation purpose which

requires lesser computational power as compared to that of original model. Some general objectives of ROM are set out below:

- The ROM results should be like the original one with a small error.
- Features (i.e observability and controllability) and structure of the model should be maintained.
- The ROM method itself should be computationally efficient.

Let us consider a case of LTI system which is given as:

$$\begin{aligned} \dot{x}(t) &= Ax(t) + Bu(t) \\ y(t) &= Cx(t) + Du(t) \end{aligned} \tag{1.2.3}$$

where $A \in \mathbb{R}^{n\times n}$, $C \in \mathbb{R}^{p\times n}$, $B \in \mathbb{R}^{n\times m}$ and $D \in \mathbb{R}^{p\times m}$. In this case, the ROM will be represented as:

$$\begin{aligned} \hat{\dot{x}}(t) &= \hat{A}\hat{x}(t) + \hat{B}u(t) \\ \hat{y}(t) &= \hat{C}\hat{x}(t) + \hat{D}u(t) \end{aligned} \tag{1.2.4}$$

where $\hat{A} \in \mathbb{R}^{r\times r}$, $\hat{B} \in \mathbb{R}^{r\times m}$, $\hat{C} \in \mathbb{R}^{p\times r}$ and $D \in \mathbb{R}^{p\times m}$. The number of states of ROM is much less than that of the full order model (i.e. $r << n$). The output of reduced model is approximation of the output of the original model ($\hat{y}(t) \approx y(t)$).

Now, let us consider a nonlinear (Quadratic-bilinear) single-input single-output (SISO) system which can be written as:

$$\begin{aligned} E\dot{x}(t) &= Ax(t) + Nx(t)u(t) + Qx(t) \otimes x(t) + Bu(t), \\ y(t) &= Cx(t), \end{aligned} \tag{1.2.5}$$

where A, E, $N \in \mathbb{R}^{n\times n}$, B, $C^T \in \mathbb{R}^n$ and $Q \in \mathbb{R}^{n\times n^2}$. $u(t) \in \mathbb{R}$ is the input, $y(t) \in \mathbb{R}$ is the output of the system and $x(t) \in \mathbb{R}^n$ is the state vector. The matrix E may or may not be singular but the pencil matrix is supposed to be regular, i.e., $\lambda E - A$ is singular only for finitely many values of $\lambda \in \mathbb{C}$ [4].

The goal of MOR is to construct ROM which has dimension $r \ll n$:

$$\begin{aligned} E_r\dot{x}_r(t) &= A_r x_r(t) + N_r x_r(t)u(t) + Q_r x_r(t) \otimes x_r(t) + B_r u(t), \\ y_r(t) &= C_r x_r(t), \end{aligned} \tag{1.2.6}$$

where $A_r, E_r, N_r \in \mathbb{R}^{r\times r}$, $B_r, C_r^T \in \mathbb{R}^r$ and $Q_r \in \mathbb{R}^{r\times r^2}$. $x_r(t) \in \mathbb{R}^r$ is the state vector of ROM. with the output $y_r(t)$ of the ROM approximately equal to output $y(t)$ of original model.

1.3 Problem Statement

As discussed earlier, models representing flow and pressure of gas distribution network at different points are large and complex. The problem is to obtain fast simulation of large scale complex models in both linear and nonlinear form using interpolatory models order reduction techniques. In particular, the problem is to explore efficient model order reduction techniques for linear systems as in (1.2.4) and quadratic bilinear systems (1.2.5) (covering reduction of both linear and nonlinear systems).

1.4 Motivation and Application

Natural gas is considered one of the most commonly utilized sources of energy in the world. The demand for natural gas has been increasing for years. There are multiple variables which effect the flow of gas in the pipeline network. The modelling and simulation of gas distribution network can analyse the effect of every variable on the flow of gas. Such analysis helps to ensure the continuous flow of gas to the consumer. The simulation of gas distribution network enable us to check the flow rate and pressure of gas at every node which help in identification of losses in the network. Flow of gas in a pipe results in the loss of pressure of gas due to friction factor. The real time simulation of gas network assist in keeping the value of compression to compensate the losses due to friction factor.

In addition to modelling and simulation of gas network as well as other energy networks(power networks and water networks), MOR has applications in several other fields such as very large scale integration (VLSI) chip design, semiconductors, conservative systems and fluid flow. Some of the areas of applications of MOR have been categorised here:

1.4.1 Thermal and Electro-Thermal Models

The development of vehicles is progressing towards electric or hybrid vehicles in which change of temperature plays vital role. The electro thermal design of the electric vehicle is of great importance [5]. If we want to design the best electrical thermal system to meet the requirements of an electric vehicle, its model requires simulation. The simulation of original electro thermal model requires high computational resources which results in generation of heat. The theory of MOR is applicable to design a model with much lower dimension known as ROM. The simulation of reduced model will use less computational resources and yet it will generate faster simulation results.

1.4.2 Convection Diffusion Models

The dynamic model of scanning electrochemical microscope (SECM) is represented by PDEs. The work in the paper [6] shows that the MOR technique works fine for the given system of partial differential equations (PDEs) . Parametric model order reduction (PMOR) technique is used here [7] for time varying system for SECM. The results of the ROM are as accurate as that of the original model.

1.4.3 Structural Mechanics and Piezoelectrical Models

In this paper [8], second order damped systems is considered. It has been shown the MOR can be applied to systems where there is linear combination of stiffness and mass matrix.

The methods of MOR can also be applied to piezoelectric simulation as well [9].

1.5 Thesis Overview

The remaining part of the dissertation is structured as: Chapter 2 presents a review of the mathematical model of the gas distribution network and the MOR techniques that can be applied to the model. Chapter 3 presents the interpolatory MOR schemes for quadratic bilinear systems. Chapter 4 presents the data driven approach of MOR for gas distribution network. In chapter 5, results and discussions are presented. The conclusion part is discussed in chapter 6.

Chapter 2

Literature Review

In the previous chapter, we discussed linear and nonlinear representation of original and reduced order model of dynamical systems. Now, we look into the different MOR techniques. MOR techniques may be categorised into two main groups which are Krylov-based methods and singular value decomposition based methods. The advantages and disadvantages of some of the methods are discussed in [10].

The SVD-based model reduction techniques use SVD to compute the ROM. In such techniques, models are truncated based on singular values in such a way that the optimality conditions in the 2-norm are met. The 2-norm is used to decide the size of ROM which will provide best approximation of the original model as per our requirement. There is another set of methods which do not depend on the singular values but instead these methods are based on moment matching which are known as Krylov based approximation methods. These methods are based on rational interpolation. Some common techniques of MOR are discussed here.

2.1 Balanced Truncation Technique

The balanced truncation method computes the transformation matrix T by decomposing the controllability and observability gramians, see [11–13]. This approach is based on the observation that only a system's greatest singular values matter. The square root approach [14], which is based on Cholesky factorization of observability and controllability gramians, is an effective way of implementing the balanced truncation method. Using SVD, V and W aka basis matrices are built. Consider a dynamical system with

state space representation given Equation (1.2.4). Assuming the dynamical system is stable, the associated Lyapunov equations for the gramians are given as:

$$AP + PA^T + BB^T = 0, \tag{2.1.1}$$

$$A^TQ + QA + C^TC = 0, . \tag{2.1.2}$$

where P is controllability gramians and Q is observability gramians of the system. We need to calculate the transformation matrix T which balances the model i..e. $P = Q = \Sigma = diag(\sigma_i)$. The transformed balanced realization along with transformed gramians are given as:

$$A' = T^{-1}AT, B' = T^{-1}B, C' = CT, D' = D, P' = T^{-1}PT^{-*}, Q' = T^*QT.$$

The transformation matrix can be found using Cholesky factorization of gramians and then applying SVD [15]. We partition the balanced realization as:

$$A' = \begin{pmatrix} A_{11} & A_{12} \\ A_{21} & A_{22} \end{pmatrix},$$

$$B' = \begin{pmatrix} B_1 \\ B_2 \end{pmatrix},$$

$$C' = \begin{pmatrix} C_1 & C_2 \end{pmatrix}.$$

The matrices of ROM in Equation (1.2.4) are $\hat{A} = A_{11}$, $\hat{B} = B_1$, $\hat{C} = C_1$ and $\hat{D} = D$. The balance truncation technique works good for model having order of few thousands due to the fact that the solving Lyapunov equations require $O(n^3)$ operations with n the size of original model. The solution of Lyapunov equation for complex systems gets very expensive, computationally. Another drawback of the balanced truncation method is that it does not guaranteed the preservation of passivity.

2.2 Proper Orthogonal Decomposition

Another method of MOR which is based on SVD is proper orthogonal decomposition (POD). This method is more common in field of Computational Fluid Dynamics (CFD). The POD is generally used to evaluate effective bases for complex systems.

In this method, the inputs which consist of essential behaviour of the system are given to a certain model which builds outputs. These outputs are called 'snapshots' which

consist of column vector [16]. These snapshots describe the state of model at some moment. Consider Y is a matrix which contains snapshots of the output and belongs to $\mathbb{R}^{m\times n}$, then there exist

$$U = (u_1, u_2, ..., u_m), \quad V = (v_1, v_2, ..., v_n), \tag{2.2.1}$$

where $U \in \mathbb{R}^{m\times m}$ and $V \in \mathbb{R}^{n\times n}$. Using singular value decomposition (SVD)

$$Y = U\Sigma V^* \quad or \quad U^*YV = \begin{pmatrix} D & 0 \\ 0 & 0 \end{pmatrix} := \Sigma \in \mathbb{R}^{m\times n}. \tag{2.2.2}$$

The Y can be written as:

$$Y = (y_1, y_2, ..., y_n) = U^d D (V^d)^T = \sum_{i=1}^{d} < u_i, y_j >_{R^m} u_i. \tag{2.2.3}$$

The columns of snapshots matrix can written in the form of linearly independent columns of U^d. This methodology of MOR consists of following steps:

1. Solve the original model which consists of nonlinearity.
2. Construct the basis matrices using SVD
3. Use Basis Matrix V to construct the ROM as:

$$V^T EV \frac{dz(t)}{dt} = V^T f(Vz(t)) + V^T Bu(t) \tag{2.2.4}$$

Model order reduction using POD generates ROMs with good approximation of the output. POD has the advantage of being able to solve nonlinear PDEs. This method works well for the fixed input, but if input keeps changing, there will be need of designing ROM every time the input changes. The disadvantage of this method is that this method is structured (input) dependent.

2.3 Interpolation Based Model Order Reduction

A dynamical system can be treated as a problem of rational interpolation in which a transfer function of a system is considered as n degree rational function $H(s)$. $H_r(s)$ represents the approximation of original transfer function with respect to H_2 norm and is known as transfer function of ROM. $H_r(s)$ is obtained by Petrov-Galerkin projection in which basis matrices(V and W) are constructed as discussed in [17]. The interpolation

based model reduction gives good approximation of model but the error in output of original and reduced model depends on the selection of interpolation points and tangential directions. Apart from this, interpolation based model order reduction is possible only if there exists original model of a physical system.

In case of linear systems (where Q and N are null matrices in (1.2.5)), there are several techniques in the literature to compute ROMs, cf., [3, 18]. Among these methods, projection-based moment-matching methods [19, 20] are well used and are recently extended to nonlinear (quadratic-bilinear systems) [21–23]. Using projection matrices $V \in \mathbb{R}^{n\times r}$ and $W \in \mathbb{R}^{n\times r}$, we approximate $x(t) \approx Vx_r(t)$ such that the Petrov-Galerkin orthogonality condition holds:

$$\begin{aligned} &W^T\Big(EV\dot{x}_r(t) - \big(AVx_r(t) + NVx_r(t)u(t) + QVx_r(t)\otimes Vx_r(t) + Bu(t)\big)\Big) = 0, \\ &y_r(t) = CVx_r(t). \end{aligned} \tag{2.3.1}$$

The projection is called one-sided projection, if $W = V$. Otherwise it is known as two sided which gives ROM of the form:

$$\begin{aligned} E_r = W^TEV, \quad A_r = W^TAV, \quad Q_r = W^TQ(V\otimes V), \quad N_r = W^TNV, \\ B_r = W^TB, \quad C_r = CV. \end{aligned} \tag{2.3.2}$$

In case of linear time invariant systems, a suitable choice of V and W, implicitly ensure moment-matching, where moments are the coefficients of the Taylor series expansion of the transfer function at some predefined shift frequencies. Thus for projection-based moment-matching, the choice of V and W depends on the transfer function of the system. However, nonlinear systems have no universal input-output representation though for some classes of nonlinear systems, including the QBDAE system, it is possible to generalise the transfer function concept by utilising the Volterra theory [24], where the input-output relationship is described by a set of high-order transfer functions. This makes the concept of moment-matching slightly complex in the nonlinear case, since the structure of the basis matrices V and W in (2.3.2) now depends on multiple high-order transfer functions. To achieve moment-matching, some simplifications are made in the literature [21, 22] for computing the ROMs. For example, [22] constructs V and W such that the moments of ROM matches the moments of the first- and second-order transfer functions. In [23], simplified forms of high-order transfer functions are derived, which

also enable the projection based techniques to match moments of high-order transfer functions. In addition, all the existing moment-matching/interpolation approaches [21–23] are based on the simplification that the interpolation points is the same for each frequency variable.

Recently a new approach [25] for QBDAEs has been worked out. The approach suggests the formation of V and W using solution of two complex matrix equations. Another approach is the extension of the Loewner framework from linear/bilinear systems [26, 27] to quadratic bilinear systems [28] . Also an indirect approach for MOR of the QBDAE system is proposed in [29], where the basis matrices are constructed from the bilinear part of the QB system. In [30], the linear-bilinear part of the system is viewed as a linear parametric system and a posteriori error bound is used to choose the interpolation points and construct the basis matrices adaptively. All these techniques are using the first two or three high-order transfer functions and their structure is different from the one identified in [22].

Chapter 3

Interpolation Based Model Order of Quadratic Bilinear Systems

There are different scenarios where the dynamics of the nonlinear system can be represented by quadratic-bilinear differential algebraic equations (QBDAEs). These include simulation of distribution networks [31], fluid flow problems [32] and nonlinear VLSI circuits [21, 33]. In addition, exact transformations can be used to represent a large set of nonlinear equations in the form of QB form [21]. Most of these applications involve large number of equations, which make simulation, control and optimization computationally inefficient. MOR is used to cater this problem.

In the paper [34], we recognize a selection of interpolation points for the QB system by applying a greedy type approach based on error bounds for QB systems inspired by the proposed error bound for linear (parametric) systems in [35]. Here we relax the restriction of using the same interpolation points for different frequency variables. The method begins with certain initial interpolation points that are modified repeatedly to find a collection of interpolation points that correspond to the maximum values of specified error bounds. We interpolate not only the original transfer function and its first derivative, but also higher derivatives, guaranteeing that the QB system is well approximated for each choice of interpolation points. The iterations terminate when the set tolerance level is achieved. The main difference from the work in [30] is that the quadratic part of the system is also involved in basis construction in the proposed framework based on a posteriori error bound for QB systems, whereas only the bilinear part is considered for the basis matrix computation in [30]. The error estimator used in

[30] only estimates the error of the linear-bilinear part.

3.1 Multivariate Transfer Functions

The Volterra series expansion of the output $y(t)$ with quantities analogous to the conventional convolution operator can be used to define the input-output representation for QB systems with single input and single output. That is,

$$y(t) = \sum_{k=1}^{\infty} \int_0^t \int_0^{t_1} \cdots \int_0^{t_{k-1}} h_k(t_1, \ldots, t_k) u(t - t_1) \cdots u(t - t_k) dt_k \cdots dt_1, \tag{3.1.1}$$

where we consider the input signal to be one-sided, i.e., $u(t) = 0$ for $t < 0$. In addition, the k-dimensional kernel of the subsystem, $h_k(t_1, \ldots, t_k)$, is assumed to be one-sided for each of the generalised impulse responses. The k-dimensional subsystem in terms of the multivariate Laplace transform can be written as,

$$Y_k(s_1, \ldots, s_k) = H_k(s_1, \ldots, s_k) U(s_1) \cdots U(s_k), \tag{3.1.2}$$

where $H_k(s_1, \ldots, s_k)$ is the multivariate transfer function of the k-dimensional subsystem. The output expression (3.1.2) has generalised transfer functions in the so-called triangular form [24]. We denote k-dimensional triangular form by $H_{tri}^{[k]}(s_1, \ldots, s_k)$. Other important types of multivariate transfer functions include the symmetric and regular forms, which are described in [24]. The relationship is given as:

$$H_{sym}^{[k]}(s_1, \ldots, s_k) = \frac{1}{n!} \sum_{\pi(\cdot)} H_{tri}^{[k]}(s_{\pi(1)}, \ldots, s_{\pi(k)}), \tag{3.1.3}$$

where all $k!$ permutations of $s_1, \ldots, s_k$ are included in the summation. Also, the triangular form can be linked to the regular form of the transfer function by following relation

$$H_{tri}^{[k]}(s_1, \ldots, s_k) = H_{reg}^{[k]}(s_1, s_1 + s_2, \ldots, s_1 + s_2 + \cdots + s_k). \tag{3.1.4}$$

The structure of generalised symmetric transfer functions can be determined using the rising exponential method, according to [24]. For the first two subsystems of the QB system (1.2.5), the form of these symmetric transfer functions can be defined as

$$\begin{aligned} H_1(s_1) &= C(s_1 E - A)^{-1} B, \\ H_2(s_1, s_2) &= C((s_1 + s_2)E - A)^{-1} B(s_1, s_2), \end{aligned} \tag{3.1.5}$$

here

$$B(s_1, s_2) =: \frac{1}{2!} N(x_1(s_1) + x_1(s_2)) + Q(x_1(s_1) \otimes x_1(s_2)), \tag{3.1.6}$$

in which $x_1(s) := (sE - A)^{-1}B$ and Q satisfies $Q(u \otimes v) = Q(v \otimes u)$ for all $u, v \in \mathbb{R}^n$. Defining $x_2(s_1, s_2) := ((s_1+s_2)E-A)^{-1}B(s_1, s_2)$, the first symmetric and second-order) symmetric transfer functions can be written as

$$\begin{aligned} H_1(s_1) &= Cx_1(s_1), \\ H_2(s_1, s_2) &= Cx_2(s_1, s_2). \end{aligned} \tag{3.1.7}$$

We explain the idea of matricization before discussing partial differentiation of these multivariate transfer functions. Matricization is the process of transforming a tensor into a matrix. In [22], the matrix $Q \in \mathbb{R}^{n\times n^2}$ is known as the mode-1 matricization of a 3 dimensional tensor $\mathcal{Q} \in \mathbb{R}^{n\times n\times n}$. The $n \times n$ components of Q are the frontal slices $\mathcal{Q}_i \in \mathbb{R}^{n\times n}$ of the tensor $\mathcal{Q}$, i.e. $Q = \begin{bmatrix} \mathcal{Q}_1 & \cdots & \mathcal{Q}_n \end{bmatrix}$. The mode-2 and mode-3 matricization can be written as

$$\begin{aligned} Q^{(2)} &= \begin{bmatrix} \mathcal{Q}_1^T & \cdots & \mathcal{Q}_n^T \end{bmatrix}, \\ Q^{(3)} &= \begin{bmatrix} vec(\mathcal{Q}_1) & \cdots & vec(\mathcal{Q}_n) \end{bmatrix}^T. \end{aligned}$$

It is noticed that the following property holds

$$w^T Q(u \otimes v) = u^T Q^{(2)}(v \otimes w), \tag{3.1.8}$$

where $v, u, w \in \mathbb{R}^n$ are arbitrary and Q holds: $Q(u \otimes v) = Q(v \otimes u)$, see [36]. Let $G(s) := sE - A$, then by using

$$\frac{\partial G(s)^{-1}}{\partial s} = -G(s)^{-1}\frac{\partial G(s)}{\partial s}G(s)^{-1},$$

and (3.1.8), we have

$$\begin{aligned} \frac{\partial H_2(s_1, s_2)}{\partial s_1} = &-y_1(s_1 + s_2)^T E x_2(s_1, s_2) \\ &- x_1(s_1)^T E^T y_2(s_1, s_2) \end{aligned} \tag{3.1.9}$$

where $y_1(s) := (sE - A)^{-T}C^T$ and $y_2(s_1, s_2) := (s_1E - A)^{-T}C(s_1, s_2)^T$ in which

$$C(s_1, s_2) = Q^{(2)}(x_1(s_2) \otimes y_1(s_1 + s_2)) + \frac{1}{2!}N^T y_1(s_1 + s_2)$$

Similarly

$$\begin{aligned} \frac{\partial H_2(s_1, s_2)}{\partial s_2} = &-y_1(s_1 + s_2)^T E x_2(s_1, s_2) \\ &- x_1(s_2)^T E^T y_2(s_2, s_1) \end{aligned} \tag{3.1.10}$$

Notice that when $s_1 = s_2 = \sigma$, the two partial differentiations are the same. This condition on interpolation points is assumed in [22] to show the moment-matching properties of the ROM. In the following, we show moment-matching in the multivariate settings where $s_1 \neq s_2$ ($s_1 = \sigma_{1i}$ and $s_2 = \sigma_{2i}$).

3.2 Moment-Matching for QBDAE

The goal of a moment-matching based reduction approach is to ensure that the high-order transfer functions are well approximated. In case of symmetric transfer functions, we can represent it as

$$H_k(s_1,\dots,s_k) \approx \hat{H}_k(s_1,\dots,s_k), \quad \text{for } k = 1,\dots,K, \tag{3.2.1}$$

with $\hat{H}_k(s_1,\dots,s_k)$ being the k-th order multivariate transfer function of the reduced system (1.2.6). With the task in (3.2.1) achieved for some K, we can expect that the output $y(t)$ is well approximated by $\hat{y}(t)$. To get recursive relations between vectors for approximation subspaces, it is assumed in [22] that $s_1 = s_2 = \sigma$. With these settings, the second-order transfer function becomes

$$H_2(\sigma,\sigma) = y(2\sigma)^T\Big(Q\left(x_1(\sigma)\otimes x_1(\sigma)\right) + Nx_1(\sigma)\Big).$$

The following Lemma summarizes the result introduced in [22].

Lemma 1. *Let the interpolation points be $\sigma_i \in \mathbb{C}$ and $\sigma_i \notin \{eig(A,E), eig(A_r,E_r)\}$, where $\Lambda(A,E)$ illustrates the generalized eigenvalues of the matrix pencil $(\lambda E - A)$. Let us assume that $E_r = W^TEV$ is nonsingular and A_r, Q_r, N_r, B_r, C_r are as in (2.3.2) with full rank matrices $V and W \in \mathbb{R}^{n\times r}$ such that*

$$\operatorname{span}(V) = \operatorname*{span}_{j=1,\dots,k}\{x_1(\sigma_j),\ x_2(\sigma_j,\sigma_j)\},$$

$$\operatorname{span}(W) = \operatorname*{span}_{j=1,\dots,k}\{y_1(2\sigma_j),\ y_2(\sigma_j,\sigma_j)\},$$

then the reduced QBDAE satisfies the following (Hermite) interpolation conditions:

$$H_1(\sigma_j) = \hat{H}_1(\sigma_j), \qquad H_1(2\sigma_j) = \hat{H}_1(2\sigma_j),$$
$$H_2(\sigma_j,\sigma_j) = \hat{H}_2(\sigma_j,\sigma_j), \quad \frac{\partial}{\partial s_i}H_2(\sigma_j,\sigma_j) = \frac{\partial}{\partial s_i}\hat{H}_2(\sigma_j,\sigma_j), \quad i = 1,2.$$

See [22] for a proof. Next, we present moment-matching properties in the multivariable settings, where $s_1 \neq s_2$.

Lemma 2. *Let $\sigma_{1i},\sigma_{2i} \in \mathbb{C}$ with $\sigma_{1i},\sigma_{2i} \notin \{\Lambda(A,E),\Lambda(A_r,E_r)\}$. Assume that $E_r = W^TEV$ is nonsingular and A_r, Q_r, N_r, B_r, C_r are as in (2.3.2) with full rank matrices $V and W \in \mathbb{R}^{n\times r}$ such that*

$$\operatorname{span}(V) = \operatorname*{span}_{i=1,\dots,k}\{x_1(\sigma_{1i}),\ x_1(\sigma_{2i}),\ x_2(\sigma_{1i},\sigma_{2i})\}$$

$$\operatorname{span}(W) = \operatorname*{span}_{i=1,\dots,k}\{y_1(\sigma_{1i}+\sigma_{2i}),\ y_2(\sigma_{1i},\sigma_{2i}),\ y_2(\sigma_{2i},\sigma_{1i})\}.$$

Then the reduced QB system holds the following:

$$H_1(\sigma_{1i}) = \hat{H}_1(\sigma_{1i}), \quad H_1(\sigma_{2i}) = \hat{H}_1(\sigma_{2i}), \quad H_1(\sigma_{1i}+\sigma_{2i}) = \hat{H}_1(\sigma_{1i}+\sigma_{2i}),$$
$$H_2(\sigma_{1i},\sigma_{2i}) = \hat{H}_2(\sigma_{1i},\sigma_{2i}), \quad \frac{\partial}{\partial s_1}H_2(\sigma_{1i},\sigma_{2i}) = \frac{\partial}{\partial s_1}\hat{H}_2(\sigma_{1i},\sigma_{2i}),$$
$$\frac{\partial}{\partial s_2}H_2(\sigma_{2i},\sigma_{1i}) = \frac{\partial}{\partial s_2}\hat{H}_2(\sigma_{2i},\sigma_{1i}).$$

The proof of the statement is similar to Lemma 1 and therefore omitted. Note that the statement in Lemma 2 reduces to Lemma 1, if $\sigma_{1i} = \sigma_{2i}$. In [34], our goal is to point out a good choice of the interpolation points σ_{1i} and σ_{2i}.

3.3 Error Bound for QBDAE's

In this section, we show how the error bound expression, derived initially in [35] for parametric LTI systems, can be extended to the quadratic-bilinear DAEs. We begin with a brief overview of the error bound for the first subsystem, as in [35] and then discuss the extension to the second subsystem of QBDAE.

3.3.1 Error bound for $H_1(s_1)$

Here the error bound provides an estimate for the error between $H_1(s_1)$ and $\hat{H}_1(s_1)$. To this end, we represent systems (the primal and the dual) as:

$$(s_1E - A)x_1(s_1) = B, \tag{3.3.1}$$
$$(s_1E - A)^T x_1^{du}(s_1) = -C^T, \tag{3.3.2}$$

respectively, where T denotes transpose of the matrix. The error bound is constructed so that it is based on residuals, which come from MOR of the systems (the primal and the dual), respectively. The matrix pair V_1 and W_1 reduce primal system, where

$$\text{span}(V_1) = \underset{i=1,\ldots,k}{\text{span}}\{x_1(\sigma_{1i})\}, \quad \text{span}(W_1) = \underset{i=1,\ldots,k}{\text{span}}\{x_1^{du}(\sigma_{1i})\}. \tag{3.3.3}$$

Hence, the reduced primal system is,

$$(s_1\hat{E}_1 - \hat{A}_1)z_1(s_1) = \hat{B},$$

where $\hat{E}_1 = W_1^T E V_1$, $\hat{A}_1 = W_1^T A V_1$, $\hat{B}_1 = W_1^T B$ and $\hat{C}_1 = CV_1$. Here $\hat{x}_1(s_1) := V_1 z_1(s_1)$ is the approximation of $x_1(s_1)$. Due to the dual relation between (3.3.1) and (3.3.2),

the dual system can be reduced by using $V_1^{du} = W_1$ and $W_1^{du} = V_1$. The reduced dual system is

$$(s_1\tilde{E}_1 - \tilde{A}_1)^T z_1^{du}(s_1) = -\tilde{C}_1^T,$$

where $\tilde{E}_1 = V_1^T E W_1$, $\tilde{A}_1 = V_1^T A W_1$, $\tilde{C}_1 = W_1^T C^T$. Also $\tilde{x}_1^{du}(s_1) := W_1 z_1^{du}(s_1)$ is the approximation of $x_1^{du}(s_1)$. The residuals associated with the reduction of systems (the primal and the dual) can be written as

$$\begin{aligned} r_1^{pr}(s_1) &= B - (s_1E - A)V_1 z_1(s_1), \\ r_1^{du}(s_1) &= -C^T - (s_1E - A)^T W_1 z_1^{du}(s_1). \end{aligned} \tag{3.3.4}$$

The following conclusion, using these numbers, gives an a posteriori upper bound on the approximation error, $|H_1(s_1) - \hat{H}_1(s_1)|$:

Theorem 1. *[35] The upper bound on the approximation of the transfer function $H_1(s_1)$ in (3.1.5) can be written as $|H_1(s_1) - \hat{H}_1(s_1)| = \Delta_1(s_1)$, where*

$$\Delta_1(s_1) := \frac{\|r_1^{du}(s_1)\|_2 \|r_1^{pr}(s_1)\|_2}{\beta_1(s_1)}, \tag{3.3.5}$$

in which $\beta_1(s_1) = \sigma_{\min}(G(s_1))$, where $\sigma_{\min}$ denotes the smallest singular value of $G(s_1)$.

3.3.2 Error Bound for $H_2(s_1, s_2)$

Analogous to $H_1(s_1)$, we write systems (the primal and the dual) as:

$$G(s_1 + s_2)x_2(s_1, s_2) = B(s_1, s_2), \tag{3.3.6}$$

$$G^T(s_1 + s_2)x_2^{du}(s_1, s_2) = -C^T, \tag{3.3.7}$$

respectively. The interpolation points for $H_1(s_1)$ can be identified through the error bound $\Delta_1(s_1)$ by using a greedy framework as presented in [35]. This means that we can select σ_{1i} for $i = 1, \ldots, r$ as the interpolation points corresponding to the maximal values of the error bound at subsequent iterations of the greedy algorithm in [35].With these interpolation points fixed for s_1, we can also express error bound for the second subsystem. The error bound is formulated based on two residuals, which result from MOR of the systems (the primal and the dual) in (3.3.6) (3.3.7), respectively. The primal system is reduced using the matrix pair V_2 and W_2, where

$$\text{span}(V_2) = \underset{j=1,\ldots,k}{\text{span}} \{x_2(\sigma_{1i}, \sigma_{2j})\}, \quad \text{span}(W_2) = \underset{j=1,\ldots,k}{\text{span}} \{x_2^{du}(\sigma_{1i}, \sigma_{2j})\}. \tag{3.3.8}$$

Consequently, the reduced primal system is

$$((s_1+s_2)\hat{E}_2-\hat{A}_2)z_2(s_1,s_2)=\hat{B}(s_1,s_2),$$

where $\hat{E}_2=W_2^TEV_2$, $\hat{A}_2=W_2^TAV_2$, $\hat{B}(s_1,s_2)=W_2^TB(s_1,s_2)$ and $\hat{C}_2=CV_2$. Similarly, the dual system is reduced using V_2^{du} and W_2^{du},

$$\text{span}(V_2^{du})=\underset{i=1,\ldots,k}{\text{span}}\{x_2^{du}(\sigma_{1i},\sigma_{2i})\},\quad \text{span}(W_2^{du})=\underset{i=1,\ldots,k}{\text{span}}\{x_2(\sigma_{1i},\sigma_{2i})\}. \tag{3.3.9}$$

The reduced dual system is

$$((s_1+s_2)\tilde{E}_2-\tilde{A}_2)^Tz_2^{du}(s_1,s_2)=-\tilde{C}_2^T,$$

where $\tilde{E}_2=(W_2^{du})^TEV_2^{du}$, $\tilde{A}_2=(W_2^{du})^TAV_2^{du}$, $\tilde{C}_2^T=(V_2^{du})^TC^T$. The residuals associated with the reduction of the primal and dual systems can be written as

$$\begin{aligned} r_2^{pr}(s_1,s_2)&=B(s_1,s_2)-((s_1+s_2)E-A)V_2z_2(s_1,s_2),\\ r_2^{du}(s_1,s_2)&=-C^T-((s_1+s_2)E-A)^TV_2^{du}z_2^{du}(s_1,s_2). \end{aligned} \tag{3.3.10}$$

With these quantities, the following result provides an a posteriori upper bound on the approximation error, $|H_2(s_1,s_2)-\hat{H}_2(s_1,s_2)|$:

Theorem 2. *The upper bound on the approximation of* $H_2(s_1,s_2)=C((s_1+s_2)E-A)^{-1}B(s_1,s_2)$ *can be written as* $|H_2(s_1,s_2)-\hat{H}_2(s_1,s_2)|=\Delta_2(s_1,s_2)$, *where*

$$\Delta_2(s_1,s_2):=\frac{\|r_2^{du}(s_1,s_2)\|_2\|r_2^{pr}(s_1,s_2)\|_2}{\beta_2(s_1,s_2)}, \tag{3.3.11}$$

in which $\beta_2(s_1,s_2)=\sigma_{\min}(G(s_1+s_2))$, *where* $\sigma_{\min}$ *indicates the smallest singular value of* $G(s_1+s_2)=(s_1+s_2)E-A$.

The derivation of the proof is identical to Theorem 1 and therefore is omitted.

3.4 Interpolation Points using Error Bounds

As discussed, the projection matrices V and W defined in Lemma 2 require a good choice of interpolation points σ_{1i} and σ_{2i} which also serve as interpolation points for MOR of the primal and dual systems in (3.3.1)-(3.3.2) and (3.3.6)-(3.3.7). In this section, we show the use of the error bound expressions derived previously to select the interpolation points.

The idea is to identify interpolation points corresponding to the maximal bound $\Delta_1(s_1)$. Assuming that σ_{1i} are the selected interpolation points for s_1, the remaining interpolation points for s_2 correspond to the maximal bound $\Delta_2(\sigma_{1i}, s_2)$ for each value of σ_{1i}.In this way, the error bound can be used iteratively to pick a worthy choice of interpolation points in a already defined sample space, starting from certain initial choice of sigma's. The selected interpolation points are then used to make and adaptively update the required basis matrices V and W, by using the multimoment-matching technique explained before. It is interesting to see that although we need to construct the ROMs for the primal and the dual systems in (3.3.1)-(3.3.2) and (3.3.6)-(3.3.7), the projection matrices for those ROMs are obtained without extra computations, since V_1, W_1 and V_2, W_2 are part of V, W by definition. Therefore, V, W can be obtained by orthogonalizing V_1 with V_2 and W_1 with W_2 as indicated in Step 9 of Algorithm 1, where a greedy framework for selecting interpolation points is presented. For an initial pair of interpolation points, the ROMs of the primal and the dual systems in (3.3.1)-(3.3.2) and (3.3.6)-(3.3.7) are constructed and the error bounds Δ_1, Δ_2 are computed. A new pair is selected such that the corresponding error bounds Δ_1 and Δ_2 are maximized at these points. With the selected interpolation points, we enrich the projection matrices V, W for MOR of the original QB system iteratively during the greedy algorithm. Finally, the reduced quadratic bilinear system is constructed using V, W that are derived upon convergence of Algorithm 1. Algorithm 1 stops when $\Delta := \Delta_1 + \Delta_2$ is below the tolerance ϵ_{tol}, where Δ includes the errors introduced by approximating the first and second transfer functions. Since the interpolation points are selected according to the error bounds Δ_1 and Δ_2, it is important that the error bounds dynamically reflect the decay of the true error with the iteration of the greedy framework. Ideally, the error bounds should be very close to the true error. Numerical tests in Chapter 5 show that the error bounds really control the true error robustly.

Chapter 4

Application of Model order Reduction to Gas Distribution Network

The behaviour of any complex system can be checked by analysing its two responses, steady state and transient response. The former is the state response other than the equilibrium position of a system while later is the response which does not change with time. For gas networks, steady state analysis can be used to estimate pressure variations, flow rates, and temperature [37]. The work of Abeysekera and Muditha in [38] is modelling of gas distribution network for analysis of nodal pressure and gas flow. In [39], the author works on optimization of model of gas distribution network where a two-stage procedure is proposed. First stage is based on optimization techniques while the second stage uses control theory to refine the solution. In [40], the equations of gas flow are used in the form of matrix in two parts which are linear and nonlinear systems. Each part is given a network topology with same input. The results are then compared using simulation software such as MATLAB.

4.1 Modelling of Gas Distribution Network

There are certain rules which need to be taken care of while modelling any real world phenomena, such as model should comply with universal physical laws and should include components of physical systems. Consider the case of gas distribution network

which when modelled should have constraints due to pipes, junctions and other passive equipments. Such models can be used to estimate the behaviour of the network at different nodes and pipes. One of the prominent research work done in [41], in which the Euler equations were used to simulate the transient behaviour of the network for different topologies. The work of Saeid Mokhatab and William A. Poe in [42] considers Bernoulli's equation to model the flow equation with assumptions that the temperature in the network remains constant at every point and "equi-height" which implies that all the pipes in the network are on same elevation. This model also investigate the efficiency factor E which shows the impact of the corrosion of pipes. The friction factor, which is represented by a dimensionless value known as the Reynolds number, is another element that plays an important role while modelling the dynamics. The Reynolds number represents whether the gas flow is turbulent or laminar. Gonzales in [43] models the unidirectional gas flow using 1D isothermal equation which uses the law conservation of mass and momentum along with elevation of pipes considered as well. In [44], the complex network is modelled using Euler equation which is set of equations consist of equation of motion, continuity and energy. Euler equation along with state equation negating the structural interactions and heterogeneity of velocity distribution is used in [45] while in [46], compressor equation is used instead of state equation. The flow velocity in this case is low as compared to speed of sound, so the inertia term is neglected. In [47], 1D isentropic Euler equation is used which takes into an account the change in flow due to friction factor as well as the gravitational effect. We observe it that most of the work carried out in the modelling and simulation of gas distribution network uses 1D Euler equation and state equation. Graph theory deals with the visualization of networks which consist of points and lines. The knowledge of graph theory traces back to early 18^{th} century in which the work of Leonhard Euler proved to be the cornerstone of the graph theory. To assess the flow and pressure of any pipe network such as gas network, graph theory comes in handy. It uses the properties of the given network to create a simplified structure of the network. The structure of the network is a graph comprised of nodes and edges where the former can be demand, supply or interconnected points and the later represents the pipes of the network. The relation of nodes' connections with edges can be represented in the form of matrix which is known as incidence matrix. In [48], graph theory is applied where nodes and edges denotes the pressure and mass flow of a pipe, respectively. Similar work has been carried out in [49]

where graph theory is used for steady state analysis of the pipe network. In the same way, graph theory can be used in PDE models as well, see [50]. Any network can be represented in the form of nodes and edges using graph theory which can be divided into three groups: gun-barrel, non-cyclic, and cyclic topologies. Unlike gun-barrel and non-cyclic systems, cyclic pipeline architecture is generally complicated and difficult to simplify. The work in [51] examines recent developments in steady state analysis in network architecture, finding that linear systems are more amenable to simulate despite the problem's complexity. Various optimization techniques have been created to cope with complexity of cyclic and non-cyclic frameworks. Dynamic programming (DP) is one of the approaches for tending to complex non-cyclic structure like the gun-barrel and tree networks, in which the solution of complex systems is determined, recursively. In [52], DP is applied to predict the parameters of the gas network considering the ideal gas conditions. The work of Hang and Ai in [53] converts the problem of complex system into the sequential problem using model predictive control optimization which proved to be efficient.

4.2 Solution of Partial Differential Equations of Gas Network

when physical world phenomena is modelled, it gets the shape of PDEs which set of mathematical equations having partial differential with respect to one or more independent variables. To find out the solutions of PDEs, it is first converted to ODEs using discretization. There are several techniques of discretization explained in [54, 55]. In [56], the author uses finite difference method (FDM) for simulation of heat transfer of diesel powered generator. The work of Peng Wang and Bo Yu in [57] models gas pipe network using equation of momentum, energy and continuity by applying adaptive implicit finite difference scheme. This paper [58] discretizes 1D isothermal equations of gas distribution network for flow and pressure of gas using finite difference method (FDM) which investigates that the smaller mesh sizes impact the accuracy of model as compared to actual data; however, computational power increases due to bigger dimension of matrices. Various schemes of finite volume (FVM) method is explored in [59] for discretization of high pressure gas distribution network which suggests that FVM is efficient for discretization of 1D isothermal equation. In [60], implicit FVM is applied

to Euler equation to predict the transient response of gas network under the assumption that inertia term and gravity term is neglected. The results proves to be efficient and stable for dynamics of gas network. In [61], Yue Qiu compares results generated by using FDM and FVM in which FVM outperforms FDM in terms of accuracy and speed. [60] also compares two discretization techniques for natural convection flow in a square cavity in which it is observed that FVM performs better than FDM. The literature suggests that Finite volume techniques work better than other techniques while discretizing the 1D isothermal Euler equation. Therefore, we carry discretization of gas network using FVM in this thesis. To represent the law of conservation of mass, momentum and energy in transportation of gas through pipeline, Euler equation is used. In this work, [43, 50, 62, 63], some assumptions are made to keep the model simple. Pipes are considered to be underground which means the temperature does not change significantly. Therefore, energy equation has been ignored here [44, 46, 64–67].

To construct a model of complex network, Let us look into the flow of gas in a pipe with cross-sectional area a, diameter d, and length of pipe L. Then, $1D$ isothermal equation can be expressed as:

$$\frac{\partial}{\partial t}\rho = -\frac{\partial}{\partial x}\varphi, \tag{4.2.1}$$

$$\frac{\partial}{\partial t}\varphi = -\frac{\partial}{\partial x}p - \frac{\partial}{\partial x}(\rho v^2) - g\rho\frac{\partial}{\partial x}h - \frac{\lambda(\varphi)}{2d}\rho v|v|, \tag{4.2.2}$$

$$p = \gamma(T)z(p,T)\rho. \tag{4.2.3}$$

The spatial domain of the given equations is $[0, L]$. The list of symbols used are given in the table: 4.1

Table 4.1: List of Symbols

Notation	Discription	Unit	Notation	Discription	Unit
p	Pressure	$\frac{Kg}{s^2m}$	g	Gravitational constant	$\frac{m}{s^2}$
h	Pipe Elevation	m	q	Mass flow	$\frac{kg}{s}$
ρ	Density	$\frac{Kg}{m^3}$	λ	Friction factor	unitless
v	Velocity	$\frac{m}{s}$	φ	Flow rate	$\frac{m^3}{s}$
L	Length	m	T	Temperature	K
a	Cross sectional area	m^2	d	Diameter	m

Equation (4.2.1) represents the law of conservation of mass while Equation (4.2.2) denotes the conservation of momentum. Equation 4.2.3 relates the pressure with density.

Since the variable of interest is mass flow, we use $q = a\varphi$ to represent the mass flow in the given set of equations. The notations of certain variables used in [61] are followed here. We consider the isothermal case where temperature remains constant throughout the network. For isothermal process, $\gamma(T) = \gamma(T_0)$ and $z(p,T) = z_0(p)$. The inertia term can be neglected due to small value which is explained in [43]

$$\frac{\partial}{\partial t}\frac{p}{z_0(p)} = -\frac{\gamma_0}{a}\frac{\partial}{\partial x}q, \tag{4.2.4}$$

$$\frac{\partial}{\partial t}q = -a\frac{\partial}{\partial x}p - \frac{\lambda(q)\gamma_0}{2da}z_0(p)\frac{q|q|}{p}. \tag{4.2.5}$$

The treatment of compressibility and friction term as explained in [68] which result in a nonlinear system. Now to simulate the model, we need to descritize it. In the Chapter 2, we noticed that FVM is better descritization technique as compared to FDM. To apply the FVM, we rewrite isothermal equations as [61]:

$$\frac{\partial}{\partial t}p + \frac{c}{a}\frac{\partial}{\partial x}q = 0, \tag{4.2.6}$$

$$\frac{\partial}{\partial t}q + a\frac{\partial}{\partial x}p + \frac{c\lambda}{2da}\frac{q|q|}{p} = 0. \tag{4.2.7}$$

The initial conditions are the initial pressure at the start of the pipe and initial mass flow at the end the pipe which are given as:

$$\begin{cases} p = p_s, & \text{at } x = 0, \\ q = q_d, & \text{at } x = L. \end{cases} \tag{4.2.8}$$

Applying FVM, the model becomes

$$\underbrace{\begin{bmatrix} M_p & \\ & M_q \end{bmatrix}}_{\mathcal{M}} \begin{bmatrix} \partial_t p \\ \partial_t q \end{bmatrix} = \underbrace{\begin{bmatrix} 0 & K_{pq} \\ K_{qp} & 0 \end{bmatrix}}_{\mathcal{K}} \begin{bmatrix} p \\ q \end{bmatrix} + \underbrace{\overbrace{\begin{bmatrix} B_q \\ 0 \end{bmatrix}}^{\text{right BC}}}_{\mathcal{B}_q} q_d + \underbrace{\overbrace{\begin{bmatrix} 0 \\ B_p \end{bmatrix}}^{\text{left BC}}}_{\mathcal{B}_p} p_s + \begin{bmatrix} 0 \\ g(p_s, p, q) \end{bmatrix} \tag{4.2.9}$$

M_p and M_q are mass matrices which are given as:

$$M_p = \begin{bmatrix} \frac{h_1+h_2}{2} & & & & \\ & \frac{h_2+h_3}{2} & & & \\ & & \ddots & & \\ & & \frac{h_{n-2}+h_{n-1}}{2} & & \\ & & & \frac{h_{n-1}}{8} & \frac{3h_{n-1}}{8} \end{bmatrix}, M_q = \begin{bmatrix} \frac{3h_1}{8} & \frac{h_1}{8} & & & \\ & \frac{h_1+h_2}{2} & & & \\ & & \frac{h_2+h_3}{2} & & \\ & & \ddots & & \\ & & & & \frac{h_{n-2}+h_{n-1}}{2} \end{bmatrix},$$

K_{pq} and K_{qp} are upper-triangular matrix and lower triangular matrix, respectively

$$K_{pq} = -\frac{c}{2}\begin{bmatrix} -\frac{1}{a_1} & \frac{1}{a_1}-\frac{1}{a_2} & \frac{1}{a_2} & & & & \\ & -\frac{1}{a_2} & \frac{1}{a_2}-\frac{1}{a_3} & \frac{1}{a_3} & & & \\ & & \ddots & \ddots & \ddots & & \\ & & & -\frac{1}{a_{n-3}} & \frac{1}{a_{n-3}}-\frac{1}{a_{n-2}} & \frac{1}{a_{n-2}} & \\ & & & & -\frac{1}{a_{n-2}} & \frac{1}{a_{n-2}}-\frac{1}{a_{n-1}} & \\ & & & & & -\frac{1}{a_{n-1}} & \end{bmatrix},$$

$$K_{qp} = -\frac{1}{2}\begin{bmatrix} a_1 & & & & & \\ a_1-a_2 & a_2 & & & & \\ -a_2 & a_2-a_3 & a_3 & & & \\ & -a_3 & a_3-a_4 & a_4 & & \\ & & \ddots & \ddots & \ddots & \\ & & & -a_{n-2} & a_{n-2}-a_{n-1} & a_{n-1} \end{bmatrix},$$

$$B_q = -\frac{c}{2}\begin{bmatrix} 0 \\ \vdots \\ 0 \\ \frac{1}{a_{n-1}} \\ \frac{1}{a_{n-1}} \end{bmatrix}, \quad B_p = \frac{1}{2}\begin{bmatrix} a_1 \\ a_1 \\ 0 \\ \vdots \\ 0 \end{bmatrix}, \tag{4.2.10}$$

where the nonlinear term is defined as:

$$g(p_s,p,q) = -\frac{c}{4}\begin{bmatrix} \frac{h_1\lambda_1}{a_1d_1}\frac{q_1|q_1|}{p_s} \\ (\frac{h_1\lambda_1}{a_1d_1}+\frac{h_2\lambda_2}{a_2d_2})\frac{q_2|q_2|}{p_2} \\ (\frac{h_2\lambda_2}{a_2d_2}+\frac{h_3\lambda_3}{a_3d_3})\frac{q_3|q_3|}{p_3} \\ \vdots \\ (\frac{h_{n-2}\lambda_{n-2}}{a_{n-2}d_{n-2}}+\frac{h_{n-1}\lambda_{n-1}}{a_{n-1}d_{n-1}})\frac{q_{n-1}|q_{n-1}|}{p_{n-1}} \end{bmatrix}. \tag{4.2.11}$$

The set of equations for single pipe after discretization get the shape of matrices in the form of state space model as shown in (4.2.9). For more than one pipe, The representation remains same but these matrices represent block matrices which is explained here [61]. The discretized analogue of pressure and mass flow for single pipe can be represented as:

$$p = \begin{bmatrix} p_2 & p_3 & \cdots & p_n \end{bmatrix}^T, \quad q = \begin{bmatrix} q_1 & q_2 & \cdots & q_{n-1} \end{bmatrix}^T.$$

It is observed in the literature that nonlinear part plays significant role only when there are several supply sources. In our case, we consider examples of unidirectional networks; therefore, we ignore the non-linearity in the system at this stage.

4.3 The Loewner Framework

In chapter 3, we explained interpolation based model order reduction of QBDAEs which requires original model to construct ROM. In most cases, the original model is not available. Hence, we develop data driven approach for construction of ROM which is known as Loewner framework. In this method, either input-output data of time domain or frequency domain is required. This method is also based polynomial interpolation.

4.3.1 Polynomial Interpolation

Let us consider the case of polynomial interpolation problem. The dataset can be represented in the form of $S = \{(x_i, f_i)|x_i, f_i \in \mathbb{R}, i = \{1, 2, ...n\}\}$, where the x_i's and f_i's represent the nodes and points, respectively. Assuming a polynomial of degree n, polynomial coefficients $c_k, k \in \{0, 1, ..., n\}$ are to be determined which satisfy following interpolation conditions

$$p(x_i) = f_i, i \in 1, 2, ...n + 1 \text{ where.} \tag{4.3.1}$$

where $p(x) = \sum_{k=0}^{n} c_k x^k$. Now, we can write (4.3.1) in the matrix form as

$$\underbrace{\begin{bmatrix} 1 & x_1 & \cdots & x_1^n \\ 1 & x_2 & \cdots & x_2^n \\ \vdots & \vdots & \ddots & \vdots \\ 1 & x_{n+1} & \cdots & x_{n+1}^n \end{bmatrix}}_{V} \begin{bmatrix} c_0 \\ c_1 \\ \vdots \\ c_n \end{bmatrix} = \begin{bmatrix} f_1 \\ f_2 \\ \vdots \\ f_{n+1} \end{bmatrix}$$

To evaluate the coefficient c_k, the inverse of matrix V will have to be calculated. Instead, we can use Lagrange polynomials. These polynomials form Lagrange basis and have degree of n. These basis can be written as:

$$\begin{aligned}
\mathscr{L}_1(x) &= \prod_{k=1,k\neq 1}^{n+1} (x - x_k) = (x - x_2)(x - x_3)\dots(x - x_{n+1}),\\
\mathscr{L}_2(x) &= \prod_{k=1,k\neq 2}^{n+1} (x - x_k) = (x - x_1)(x - x_3)\dots(x - x_{n+1}),\\
&\vdots\\
\mathscr{L}_{n+1}(x) &= \prod_{k=1,k\neq n+1}^{n+1} (x - x_k) = (x - x_1)(x - x_3)\dots(x - x_n).
\end{aligned}$$

From this we can write $\mathscr{L}_i(x_k) = 0, \forall\ k \neq i,\ k, i, \in \{1, 2, \dots, n+1\}$. Now, polynomial p can be constructed from this basis which satisfies the (4.3.1).

$$p(x) = \sum_{i=1}^{n+1} \frac{f_i}{\mathscr{L}_i(x_i)} \mathscr{L}_i(x) = \sum_{i=1}^{n+1} b_i \mathscr{L}_i(x), \tag{4.3.2}$$

where

$$b_i = \frac{f_i}{\mathscr{L}_i(x_i)},$$

which can be calculated using given datasets. Using different basis can give different form of polynomial. The use of Lagrange polynomial instead of monomial polynomial is to avoid the solution of large ill-conditioned linear system as explained here [69]. Let us define another polynomial $g(x)$ of degree n using the Lagrange polynomial. The $g(x)$ can be represented as:

$$g(x) = \sum_{i=1}^{n+1} \frac{1}{\mathscr{L}_i(x_i)} \mathscr{L}_i(x) \tag{4.3.3}$$

From (4.3.3), we can write $g(x_i) = 1,\ \forall\ i \in \{1, 2, \dots, n+1\}$ as represented in [70]. Let polynomial $P(x) = \frac{p(x)}{g(x)}, \forall x \in \mathbb{R}$, then using (4.3.2) and (4.3.3), the baryscentric formula for rational polynomial is:

$$P(x) = \frac{\sum_{i=1}^{n+1} \frac{f_i}{\mathscr{L}_i(x_i)} \mathscr{L}_i(x)}{\sum_{i=1}^{n+1} \frac{1}{\mathscr{L}_i(x_i)} \mathscr{L}_i(x)} \tag{4.3.4}$$

4.3.2 Rational Lagrange Interpolation

The rational function is the ratio between two polynomials which can be written as:

$$r(x) = \frac{N(x)}{D(x)} = \frac{\beta_n X^n + \beta_{n-1} X^{n-1} + \ldots + \beta_1 X^1 + \beta_0}{\alpha_n X^n + \alpha_{n-1} X^{n-1} + \ldots + \alpha_1 X^1 + \alpha_0}, \tag{4.3.5}$$

where $\beta_k, \alpha_k \in \mathbb{R}, k \in \{0, 1, \ldots, n\}$ and also $\beta_n, \alpha_n \neq 0$. The polynomial $N(x)$ is said to be numerator polynomial while the polynomial $D(x)$ is called denominator of the rational function $r(x)$. As the roots of numerator and denominator represent zeros and poles of the function, respectively; hence, the rational function represents transfer function of the complex dynamical systems. The complex exponential function can also be written in the form rational function while dealing with it in the frequency domain.

we have seen in (4.3.1) that $n+1$ pairs of data set are required to construct n^{th} order polynomial. So, in order to recover the rational function $r(x)$ with two polynomials, $2(n+1)$ pairs of sampling points will be required; however, the coefficient α_n of the rational function in (4.3.5) can be set to 1 by dividing and multiplying the rational function with α_n which will develop new set of coefficients $\hat{\alpha} = \frac{\alpha_k}{\alpha_n}$ and $\hat{\beta} = \frac{\beta_k}{\alpha_n}$. To compute rational interpolants of order n , $2n+1$ coefficients are required so that following conditions are satisfied

$$r(x_h) = f_h \quad h \in \{1, 2, \ldots, 2n+1\}.$$

Let's partition the set of interpolation nodes into disjoint sets:

$$\{x_1, x_2, \ldots, x_{2n+1}\} = \{\mu_1, \mu_2, \ldots, \mu_n\} \cup \{\lambda_1, \lambda_2, \ldots, \lambda_{n+1}\},$$

similarly, partition the set of interpolation points into disjoint sets:

$$\{f_1, f_2, \ldots, f_{2n+1}\} = \{\upsilon_1, \upsilon_2, \ldots, \upsilon_n\} \cup \{w_1, w_2, \ldots, w_{n+1}\}.$$

We use the Lagrange basis and the barycentric formula to rephrase the rational interpolation problem as:

$$r(x_h) = f_h, \quad h \in \{1, 2, \ldots, 2n+1\} \; where \; r(x) = \frac{\sum_{i=1}^{n+1} b_i \mathscr{L}_i(x)}{\sum_{i=1}^{n+1} a_i \mathscr{L}_i(x)} \tag{4.3.6}$$

where $\mathscr{L}_i(x) = \prod_{k=1, k\neq i}^{n+1} (x - \lambda_k)$, $i \in \{1, 2, \ldots, n+1\}$ are Lagrange polynomials . We need to obtain the coefficients a_i and b_i to recover the function $r(x)$ such that

$r(\mu_j) = \upsilon_j, j \in \{1, 2, \ldots, n\}$, $r(\lambda_i) = w_i, i \in \{1, 2, \ldots, n+1\}$ Since, $\mathscr{L}_j(\lambda_i) = 0, \forall j \neq i$, evaluating equation (4.3.6) will give us:

$$r(\lambda_i) = \frac{b_i}{a_i} \Rightarrow w_i = \frac{b_i}{a_i} \Rightarrow b_i = w_i a_i, \forall i \in \{1, 2, \ldots, n+1\}$$

$r(x)$ can alternatively be written as:

$$r(x) = \frac{\sum_{i=1}^{n+1} \frac{w_i a_i}{x - \lambda_i}}{\sum_{i=1}^{n+1} \frac{a_i}{x - \lambda_i}}. \tag{4.3.7}$$

4.3.3 The Loewner Matrix

Using rational functional $r(x)$ used in equation (4.3.7) for $r(\mu_j) = \upsilon_j$, we get:

$$\sum_{j=1}^{n} \sum_{i=1}^{n+1} \frac{\upsilon_j - w_i}{\mu_j - \lambda_i} a_i = 0, \Leftrightarrow \mathbb{L}a = 0,$$

The Loewner Matrix can be defined as:

$$\mathbb{L} = \begin{bmatrix} \frac{\upsilon_1 - w_1}{\mu_1 - \lambda_1} & \frac{\upsilon_1 - w_2}{\mu_1 - \lambda_2} & \cdots & \frac{\upsilon_1 - w_{n+1}}{\mu_1 - \lambda_{n+1}} \\ \frac{\upsilon_2 - w_1}{\mu_2 - \lambda_1} & \frac{\upsilon_2 - w_2}{\mu_2 - \lambda_2} & \cdots & \frac{\upsilon_2 - w_{n+1}}{\mu_2 - \lambda_{n+1}} \\ \vdots & \vdots & \ddots & \vdots \\ \frac{\upsilon_n - w_1}{\mu_n - \lambda_n} & \frac{\upsilon_n - w_2}{\mu_n - \lambda_2} & \cdots & \frac{\upsilon_n - w_{n+1}}{\mu_n - \lambda_{n+1}} \end{bmatrix} \in \mathbb{R}^{n \times (n+1)} \tag{4.3.8}$$

Null space of $\mathbb{L}$ gives us: $a = [a_1 \ a_2 \ \ldots \ a_{n+1}]^T$. Next, we find $b_i = w_i a_i$, $\forall$ $i \in \{1, 2, \ldots, n+1\}$

4.3.4 The Loewner Pencil

We consider frequency response data of linear system and divide it into two disjoint sets represented by left response data and right response data. The left data is represented by $\{\mu_j\}_{j=1}^{q} \subset \mathbb{C}$ with left input tangential direction $\{l_j\}_{j=1}^{q} \subset \mathbb{C}^p$ which gives left responses $\{v_j\}_{j=1}^{q} \subset \mathbb{C}^m$. Similarly, right data is represented by $\{\lambda_j\}_{i=1}^{k} \subset \mathbb{C}$ with right input tangential direction $\{r_j\}_{i=1}^{k} \subset \mathbb{C}^m$ which gives right responses $\{w_i\}_{j=1}^{k} \subset \mathbb{C}^p$ which can be represented as

$$l_j^T \hat{H}(\mu_j) = v_j^T, \quad j = 1, \ldots, q, \text{ and } \hat{H}(\lambda_i) r_i = w_i, \quad i = 1, \ldots, k. \tag{4.3.9}$$

Now, let $\mathcal{R}$ and $\mathcal{O}$ be generalised controllability and observability matrices, respectively for the given linear model $\Sigma_L = (C, E, A, B)$ of order n, then the associated Loewner

matrix is given as:

$$\mathbb{L} = \begin{bmatrix} \frac{v_1^T r_1 - \ell_1^T w_1}{\mu_1 - \lambda_1} & \cdots & \frac{v_1^T r_k - \ell_1^T w_k}{\mu_1 - \lambda_k} \\ \vdots & \ddots & \vdots \\ \frac{v_q^T r_1 - \ell_q^T w_1}{\mu_q - \lambda_1} & \cdots & \frac{v_q^T r_k - \ell_q^T w_k}{\mu_q - \lambda_k} \end{bmatrix} = -\mathcal{O}E\mathcal{R} \tag{4.3.10}$$

The shifted Loewner matrix is:

$$\mathbb{L}_s = \begin{bmatrix} \frac{\mu_1 v_1^T r_1 - \ell_1^T w_1 \lambda_1}{\mu_1 - \lambda_1} & \cdots & \frac{\mu_1 v_1^T r_k - \ell_1^T w_k \lambda_k}{\mu_1 - \lambda_k} \\ \vdots & \ddots & \vdots \\ \frac{\mu_q v_q^T r_1 - \ell_q^T w_1 \lambda_1}{\mu_q - \lambda_1} & \cdots & \frac{\mu_q v_q^T r_k - \ell_q^T w_k \lambda_k}{\mu_q - \lambda_k} \end{bmatrix} = -\mathcal{O}A\mathcal{R} \tag{4.3.11}$$

The controllability and observability matrices are explained in [70]. The matrix $[\mathbb{L}, \mathbb{L}_s]$ is known as Loewner Pencil and transfer function of raw model will be written as:

$$H(s) = \mathbf{W}(\mathbb{L}_s - s\mathbb{L})^{-1}\mathbf{V} \tag{4.3.12}$$

Consider given frequency domain measurments $(s_i, H(s_i))$. Partiition the measurement into two disjoint sets

$$frequencies: \quad [s_1, \ldots, s_N] \;=\; [\lambda_1, \ldots, \lambda_k],\ [\mu_1, \ldots, \mu_q],\ k + q = N,$$

$$values: \quad [H(s_1), \ldots, H(s_N)] \;=\; [w_1, \ldots, w_k],\ [v_1, \ldots, v_q] = W, V^T.$$

Build the Loewner matrix pencil $(\mathbb{L}, \mathbb{L}_s)$ using (4.3.10) and (4.3.11). Next, compute the SVDs

$$[\mathbb{L}, \mathbb{L}_s] = Y_1 \Sigma_\ell \widetilde{X}_1^T, \begin{bmatrix} \mathbb{L} \\ \mathbb{L}_s \end{bmatrix} = \widetilde{Y_2} \Sigma_r X_2^* \tag{4.3.13}$$

If we have the case of redundant data, then Loewner pencil $(\mathbb{L}, \mathbb{L}_s)$ is singular and following assumption is made

$$rank(x\mathbb{L} - \mathbb{L}_s) = rank[\mathbb{L}; \mathbb{L}_s] = rank[\mathbb{L}, \mathbb{L}_s] = r \leqslant k.$$

The reduced order model $(\widehat{C}, \widehat{E}, \widehat{A}, \widehat{B})$ is obtained by projecting the raw model $(W, \mathbb{L}, \mathbb{L}_s, V)$ onto subspace of dimension r . By selecting r columns of Y_1 and X_2 , we get projection matrices of size $Y, X \in \mathbb{C}^{r \times k}$. The following relationship holds in general

$$\widehat{E} = -Y^* \mathbb{L} X,\ \widehat{A} = -Y^* \mathbb{L}_s X,\ \widehat{B} = -Y^* V,\ \widehat{C} = WX.$$

This methodology is used to construct ROM of gas distribution network using the frequency response data of network model on certain interpolation points.

4.4 Graphical User Interface

In this thesis, we built a classic GUI with MATLAB AppDesigner which is used to simulate different network. The interface of the design is shown in Figure 4.1

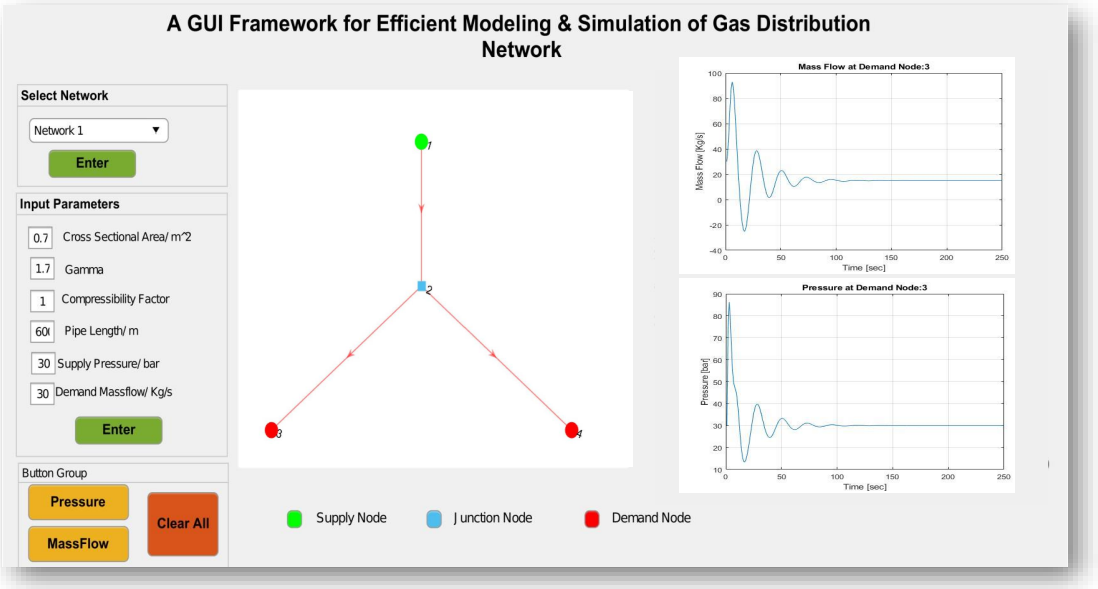

Figure 4.1: Graphical User Interface

The input parameters defined in the GUI is explained here:

- **Select Network:** This drop down bar is used to choose the desired network. For gas network, the nodes defined by number can be entered to our model by defining it in the form of source and target array in which each element represents the pipe from source to target.
- **Cross sectional area:** It represents the cross sectional area of each pipe in the form of row vector. The first element represents the area of first pipe and so on.
- **Supply pressure and demand mass flow:** These parameters are also used as boundary conditions in the model. For multiple demand or supply nodes, the data will be entered in the form of row vector.
- **Length of pipes:** The length of more than one pipe is entered in the form of row vector with first element represents length of first pipe and so on.

- **Compressibility factor and gamma:** In ideal case, we consider the compressibility factor as one while gamma represents ratio of specific heat.
- **Choose node:** We choose node to check the pressure and mass flow at the required node. The graph of mass flow and pressure will be displayed on the given figures in the GUI.

Chapter 5

Results and Discussion

We consider three benchmark examples for our results on MOR of QBDAE systems. The results are compared with the one-sided and two-sided projection methods, where the interpolation points are computed by IRKA, implemented on the linear part of the system. We represented the proposed method by 1s/2s-greedy(One-sided/two-sided projection with greedy based interpolation points) and the method from literature by 1s/2s-IRKA (One-sided/two- sided projection with IRKA interpolation points). The Max. True error in the following tables is defined as $\max_{s_1,s_2\in S_{\text{sample}}} |H_1(s_1)-\hat{H}_1(s_1)|+|H_2(s_1,s_2)-\hat{H}_2(s_1,s_2)|$ and the Max. error bound is $\max_{s_1,s_2\in S_{\text{sample}}} \Delta(s_1,s_2)$. Next, we try Loewner framework on linear time invariant dynamical system of gas distribution network. Three different scheme of gas network is considered to validate our methodology in 4 for various network schemes.

5.1 Nonlinear RC circuit

The nonlinear RC circuit was first considered in [71] and since then it has been used in many papers for nonlinear MOR [4]. Consider v be the voltage and $g(v)$ be the current function then I-V characteristics can be represented as: $g(v) = e^{40v} + v - 1$. The nonlinearity in the current function results in nonlinear model. All the capacitances are fixed to $C = 1$. Figure 5.1 shows the complete circuit.

It is shown in [21] that introducing some auxiliary variables, the nonlinearity in the RC circuit can be written in the QB form as in (1.2.5). The transformation is exact, but the dimension of the system increases to $n = 2 \cdot l$, where l represents the number of nodes

in Figure 5.1, and it is also the dimension of the original nonlinear system.

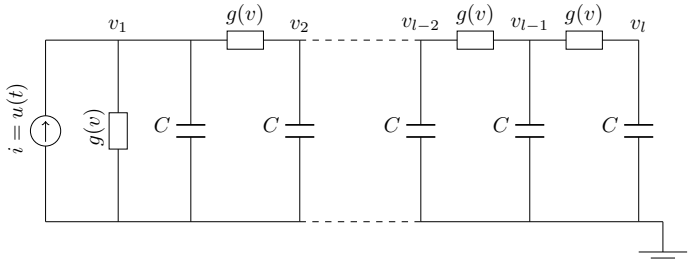

Figure 5.1: Nonlinear RC circuit diagram

For our results, we set $l = 50$, so $n = 100$ and use two-sided projection method to reduce the system. Table 5.1 shows the results with tolerance $\epsilon_{tol} = 1e^{-5}$ and an initial choice of interpolation points as $\sigma_1 = \sigma_{20} = 119.5642$.

S.No.	Interpolation points $\{\sigma_{1i}, \sigma_{2i}\}$	Max. True Error	Max. Est. Error
1	$119.5642, 119.5642$	1.8616×10^{-2}	0.109183
2	$0.9875, 0.9875$	1.3683×10^{-3}	8.4421×10^{-3}
3	$4.9567, 0.9875$	1.6127×10^{-4}	4.0341×10^{-4}
4	$18.1107, 5.5319$	4.2956×10^{-5}	7.22×10^{-5}
5	$2.0292, 4.4445$	8.239×10^{-6}	9.6404×10^{-6}

Table 5.1: Error estimation results for RC circuit

The second column of Table 5.1 shows interpolation points that are identified by the greedy framework and are based on the error bound. It is clear that the error bound tightly catches the true error and can be used as a surrogate of the true error to select the interpolation points. The size of the ROM obtained from both approaches has been kept the same i.e. $r_1 = r_2 = 12$. For the input $u(t) = e^{-t}$, the output of the original model and ROMs along with corresponding relative errors are shown in Figure 5.2.

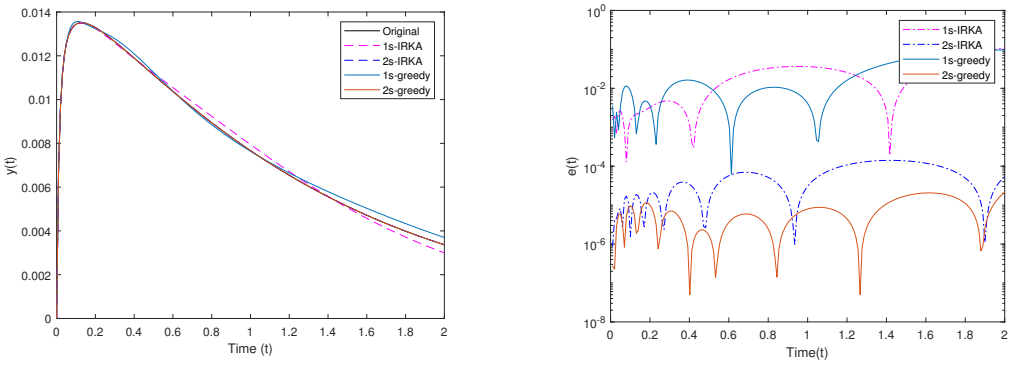

(a) Comparison of transient response

(b) Comparison of relative error

Figure 5.2: Non-linear RC circuit

Figure 5.2a shows the comparison of transient response of the two approaches, while Figure 5.2b plots relative errors of the two approaches. It is clearly seen that 1s-greedy and 2s-greedy outperform 1s-IRKA and 2s-IRKA respectively in terms of accuracy.

5.2 Burgers' Equation

In nonlinear MOR, 1D burgers' equation is commonly used [32],[22]. Mathematical model of 1D burger's equation with $\Gamma = (0,1) \times (1,T)$ is:

$$\begin{aligned} \upsilon_t + \upsilon\upsilon_x &= \nu \cdot \upsilon\upsilon_{xx}, && in\ \Gamma, \\ \alpha\upsilon(0,t) + \beta x(0,t) &= u(t), \quad \upsilon_x(1,t) = 0, && t \in (0,T), \\ \upsilon(x,0) &= \upsilon_0(x), \quad \upsilon_0(x) = 0, && x \in (0,1), \end{aligned} \tag{5.2.1}$$

we use it as an example to test our proposed method. We keep the size of the original model as n = 1000. Table 5.2 shows our results with tolerance $\epsilon_{tol} = 1e^{-4}$ and an initial choice of interpolation points as $\sigma_{10} = \sigma_{20} = 5.4124$.

S.No.	Interpolation points $\{\sigma_{1i}, \sigma_{2i}\}$	Max. True Error	Max. Est. Error
1	$5.4124, 5.4124$	1.1299×10^{-3}	32.4786
2	$31.6141, 1.383$	1.0259×10^{-3}	3.2407
3	$2.9603, 1.0818$	1.0746×10^{-3}	4.2125×10^{-1}
4	$9.2633 - 11.3351\iota, 24.9534$	1.416×10^{-4}	4.3411×10^{-4}
5	$7.4119 - 3.622\iota, 1.0818$	1.785×10^{-5}	1.7869×10^{-5}

Table 5.2: Error estimation results for burgers equation

The second column of the table shows interpolation points that are based on the error bound and identified by the greedy framework. Similarly, the error bound again tightly bounds the true error and therefore is reliable for choosing the interpolation points in the greedy algorithm. The sizes of the ROMs obtained from both approaches are kept same i.e. $r_1 = r_2 = 16$. The ROMs constructed from IRKA interpolation points and the proposed framework are shown in Figure 5.3 for input $u(t) = cos(\pi t)$.

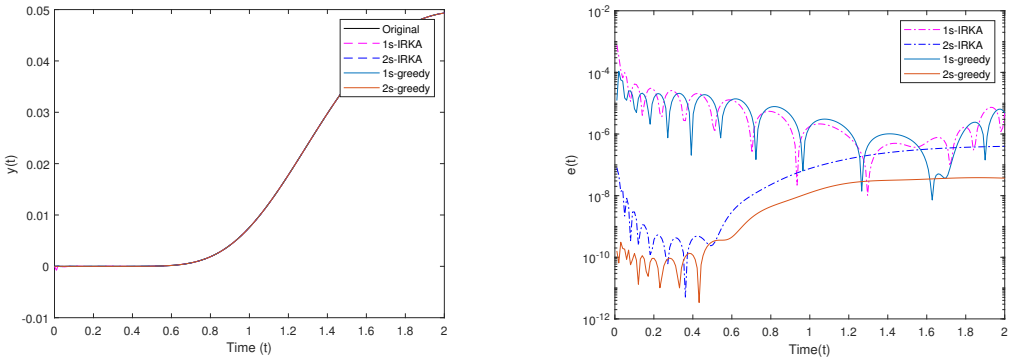

(a) Comparison of transient response

(b) Comparison of absolute error

Figure 5.3: Burger's equation

Figure 5.3a shows the transient responses of the burgers equation computed from simulating the original model and the two different MOR approaches, while Figure 5.3b compares the absolute response errors of the ROMs derived using two approaches. The absolute error of ROM constructed using the proposed methodology of choosing interpolation points is less than that of the ROM constructed using IRKA interpolation points, especially for the two-sided projection.

5.3 FitzHugh - Nagumo System

We use the FitzHugh - Nagumo system as our third example to check our results. The FitzHugh - Nagumo system can be represented as[25]:

$$\begin{aligned} \epsilon v_t(x,t) &= \epsilon^2 v_{xx}(x,t) + f(v(x,t)) - w(x,t) + g, \\ w_t(x,t) &= hv(x,t) - \gamma w(x,t) + g, \end{aligned} \tag{5.3.1}$$

with $f(v) = v(v-0.1)(1-v)$ and boundary conditions:

$$\begin{aligned} v(x,0) &= 0, & w(x,0) &= 0, \\ v_x(0,t) &= -i_0(t), & v_x(1,t) &= 0. \end{aligned} \tag{5.3.2}$$

Here, we choose $\epsilon = 0.015$, $h = 0.5$, $\gamma = 0.05$ and $i_0(t) = 5 \times 10^4 t^3 e^{-15t}$. When standard finite difference method is applied to numerically discretize the PDEs in (5.3.1), a system of ODEs with cubic non-linearities is obtained. We can get a quadratic bilinear system by introducing new variables. For an original discretized system with size $\bar{n}$, a quadratic bilinear system has the size of $n = 3\bar{n}$. we set $\bar{n} = 100$, which gives rise to quadratic bilinear system of $n = 300$. We choose interpolation points using the proposed greedy framework to construct the ROM of size $r = 26$ and then compare it with the ROM of the same size, which is constructed from the interpolation points using IRKA. Table 5.3 shows our results with tolerance $\epsilon_{tol} = 1e^{-6}$ and the interpolation points $\sigma_{10} = \sigma_{20} = 534.69$.

S.No.	Interpolation points $\{\sigma_{1i}, \sigma_{2i}\}$	Max. True Error	Max. Est. Error
1	$534.69, 534.69$	0.282519	1152.4511
2	$1.38, 1.08$	4.7413×10^{-1}	8.4587
3	$3.91 - 5.45\iota, 1.38$	1.2373×10^{-4}	4.3284×10^{-3}
4	$39.38, 1.08$	2.5379×10^{-6}	5.9555×10^{-5}
5	$110.46, 1.08$	8.2393×10^{-6}	2.1293×10^{-5}
6	$3.96, 1.08$	4.3429×10^{-5}	7.1251×10^{-4}
7	$17.63, 1.08$	7.6047×10^{-6}	4.6707×10^{-5}
8	$4.83 - 4.72\iota, 1.08$	9.7775×10^{-8}	1.932×10^{-7}

Table 5.3: Error estimation results for the FitzHugh - Nagumo model

The table 5.3 shows interpolation points that are selected by the error bound and the decay of the true error and the error bound at each iteration of the greedy algorithm. The error bound once more, estimates the true error accurately, implicating that the selected interpolation points indeed nearly corresponds to the largest error. The sizes of ROMs obtained from both approaches have been kept the same i.e. $r_1 = r_2 = 26$. Figure 5.4 shows the transient responses of the FitzHugh - Nagumo system computed from simulating the original model and two approaches.

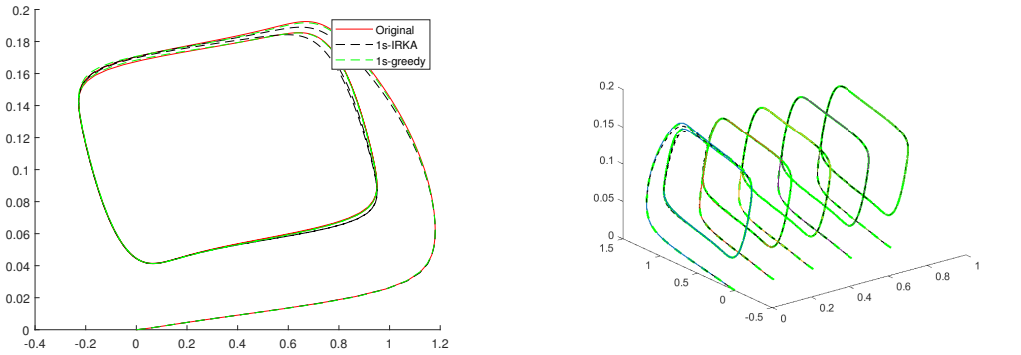

(a) Comparison of transient response

(b) Comparison of transient response (3D)

Figure 5.4: FitzHugh - Nagumo equation

The input signal is $u(t) = 50000t^3e^{-15t}$. It is seen that the 1s-greedy performs better than the 1s-IRKA when the outputs in both cases are compared with that of the original model; however, 2s-greedy and 2s-IRKA produce unstable responses.

5.4 Simple Fork Network

This section covers two different cases of fork network. The following setting has been considered for simulation of these networks:

1. Each pipe has length which is measured in meter [m]. The length of pipes may vary.

2. Each pipe has its own diameter. The cross sectional areas of each pipe is calculated using the diameter of the pipe.

3. Gamma which represents the specific heat capacity of the gas is taken as constant.

4. The compressibility factor is considered fixed such as unity for ideal gas.

5.4.1 Fork Network 1

This network consists of three pipes. There are one supply node, two demand nodes and one junction node. The network is plotted using digraph as shown in the Figure 5.5.

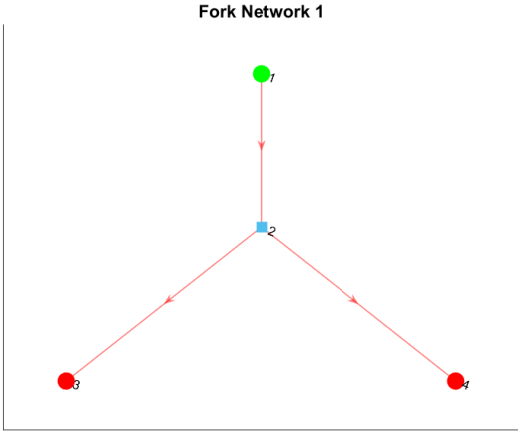

Figure 5.5: Simple Gas Fork Network 1

The pipe connected to supply node is known as supply pipe while the pipe connected to demand node is called demand pipe which mean that the flow of gas at certain node represents the flow in the corresponding pipe. The input data of the model is given in the Table 5.4.

Table 5.4: Given Data of Fork Network 1

Description	Symbol	Value
Pressure at 1^{st} supply node	p_{s1}	30 bar
Flow rate at 1^{st} demand node	q_{d1}	30 kg/s
Flow rate at 2^{nd} demand node	q_{d2}	30 kg/s
Area of each pipe	a	0.7854 m^2
Gamma	γ	1.46745319
Compressibility Factor	c	1
Mesh size	h	20
Length of each pipe	L	1000 m

With the above input parameters for the simulation of the network in the 5.5, we choose

the simulation time $t = 1000$ *seconds*. We consider frequency response data of original transfer function at $2n$ different interpolation points where n represents the size of the original system. These interpolation points are used to construct ROM. To simulate the models, we keep the initial condition as zero. The simulation of FOM and ROM generate results with very small error. The flow rates at demand nodes generated by original and reduced order model can be seen in Figure 5.6.

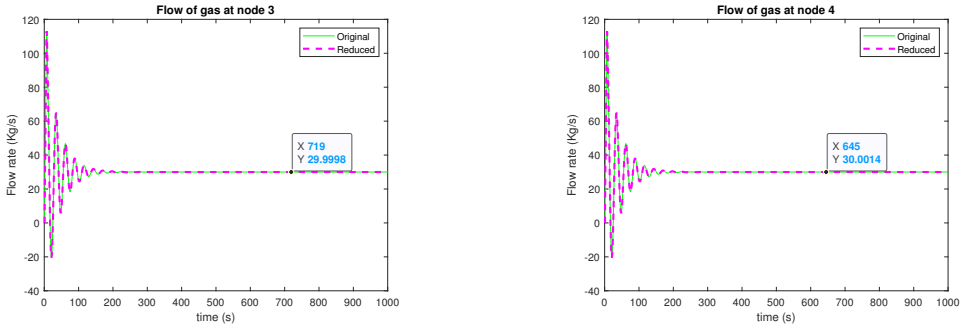

Figure 5.6: Fork Network 1 Flow Rates at Demand Nodes

While Figure 5.7 represents the flow rate at supply node in the network.

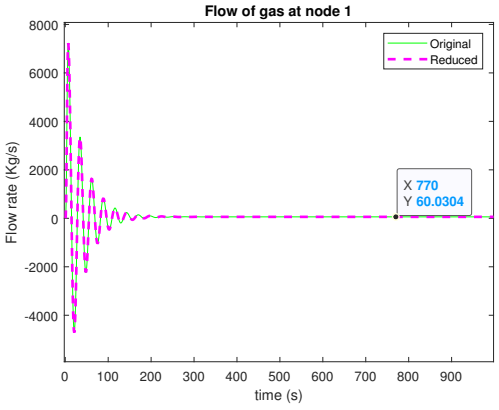

Figure 5.7: Fork Network 1 Flow Rate at Supply Node

Similarly, the pressure at each node can be seen as well. The pressures at demand nodes are given in Figure 5.8

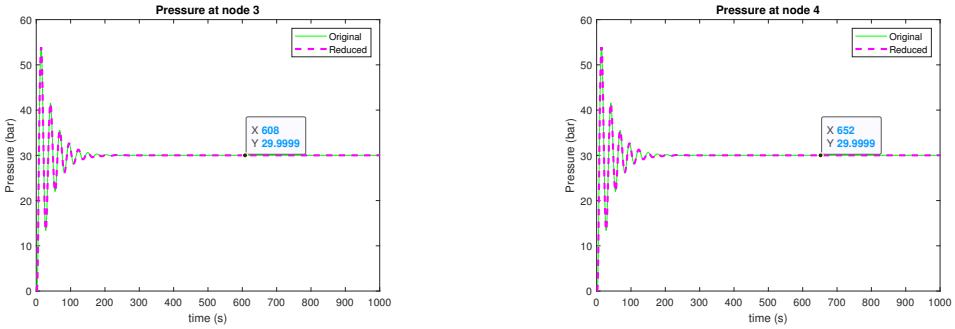

Figure 5.8: Fork Network 1 Pressure at Demand Nodes

Next, the pressure at supply node is plotted in Figure 5.9

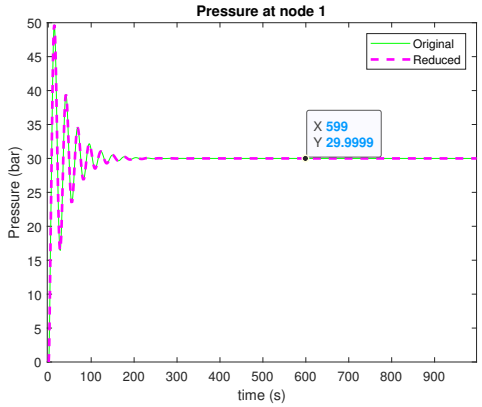

Figure 5.9: Fork Network 1 Pressure at Supply Node

Now, we need to check the accuracy of the results generated from reduced order model. The relative error at every point is given in Figure 5.10

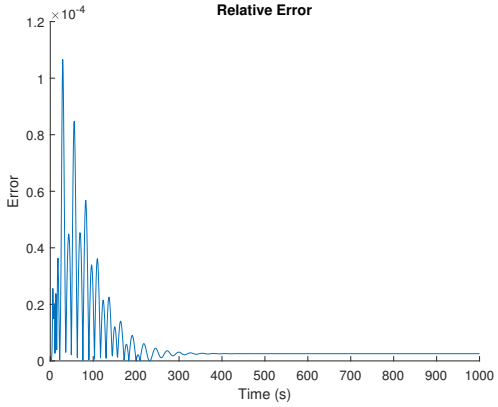

Figure 5.10: Fork Network 1 Relative Error

It is observed that our results from ROM closely match the results of FOM with a small acceptable error in our case. The size of the original system is $n = 301$ while the size of the reduced model is $r = 18$. Therefore, the simulation time of original model is 0.9304 *seconds* while that of the ROM is 0.0979 *seconds*. Simulation of ROM takes approximately 89.47% less time as compared to original model which save our computational resources as well. Apart from this, the reduced order model works fine with variable inputs as well.

5.4.2 Fork Network 2

This network also consists of three pipes. However two sources of gas supply are considered. The network consists of single demand node. The network is displayed using directed graph as shown in the Figure 5.11.

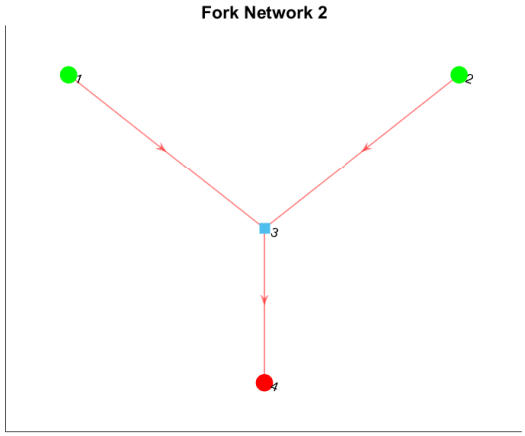

Figure 5.11: Simple Gas Fork Network 2

In this case, we have two supply pipes and single demand pipe. The input data of the model is given in the Table 5.5.

Table 5.5: Given Data of Fork Network 2

Description	Symbol	Value
Pressure at 1^{st} supply node	p_{s1}	30 bar
Pressure at 2^{nd} supply node	p_{s2}	30 bar
Flow rate at 1^{st} demand node	q_{d1}	30 kg/s
Area of each pipe	a	0.7854 m^2
Gamma	γ	1.46745319
Compressibility Factor	c	1
Mesh size	h	20
Length of each pipe	L	1000 m

With the above input parameters for the simulation of the network in the 5.11, we choose the simulation time $t = 1000$ *seconds*. We consider frequency response data of original transfer function at $2n$ different interpolation points where n represents the size of the original system. we keep the interpolation points same as in 5.4.2. These interpolation points along with frequency response at these points are used to construct ROM. We simulate both the models with zero initial conditions. The simulation of ROM generates results, closely match with that of FOM. The flow rates at supply nodes generated by original and reduced order model can be seen in Figure 5.12.

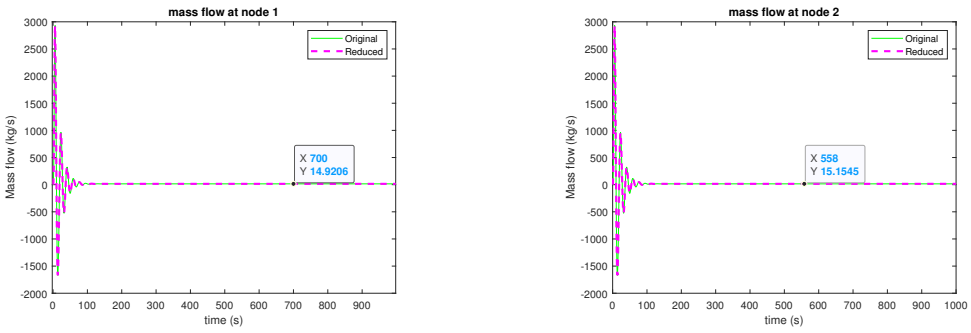

Figure 5.12: Fork Network 2 Flow Rate at Supply Nodes

While Figure 5.13 represents the flow rate at demand node in the network.

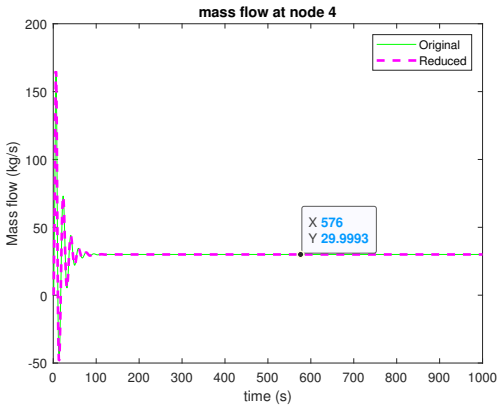

Figure 5.13: Fork Network 2 Flow Rate at Demand Node

Similarly, the pressure at each node can be seen as well. The pressure at supply nodes are given in Figure 5.14

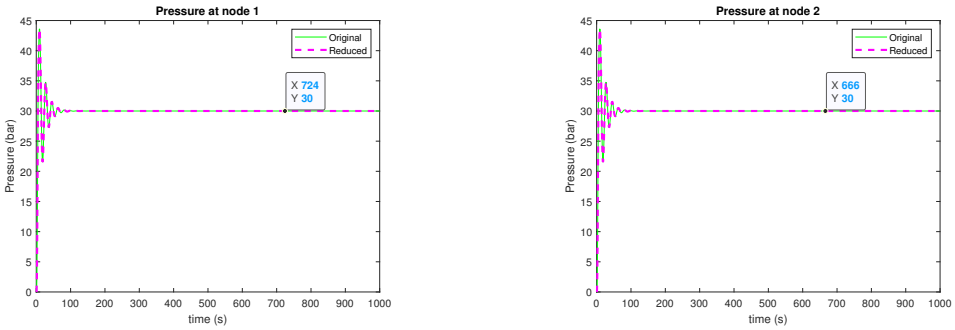

Figure 5.14: Fork Network 2 Pressure at Supply Nodes

Next, the pressure at demand node is plotted in Figure 5.15

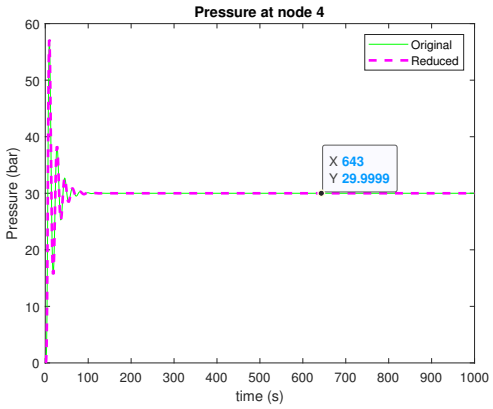

Figure 5.15: Fork Network 2 Pressure at demand Node

Now, we need to look how accurately constructed ROM generates results as compared to original model. The relative error at every point is given in Figure 5.16

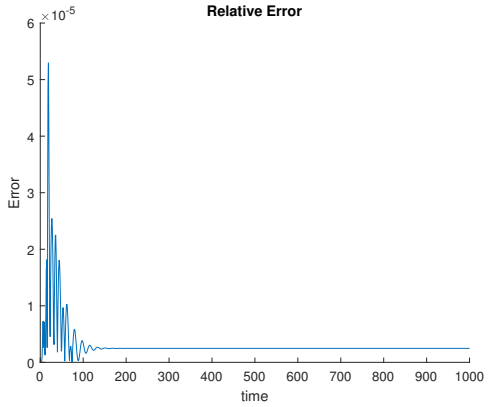

Figure 5.16: Fork Network 2 Relative Error

Since we know the network has two supply sources, we see in Figure 5.6 that mass flow in steady state at each supply node is same. It is because the pressure of both supply nodes are same. In case the pressure is not same, then supply node with lower pressure act as demand node. It is also observed that our results from ROM closely matches the results of original model with a small error. The size of the original is $n = 302$ while the size of the ROM is $r = 12$. Therefore, the simulation time of original model is 1.2359 *seconds* while that of the ROM is 0.0635 *seconds*. Simulation of ROM takes approximately 94.86% less time as compared to original model which save our computational power as well. Apart from this, the ROM works fine with variable inputs as well.

5.5 Cyclic Network

In this section, a simple gas network with cyclic struture will be used to apply data driven model reduction and compare results with original model with same length and cross section area for all pipes. Later on, the MOR technique will be applied to original model with different length and corss sectional area for each pipe. We will see the effectiveness of our methodology which works even for different possible cases of a network.

5.5.1 Simple Cyclic Network

We consider a basic structure of cyclic network and keep same settings defined in Section 5.4. The directed graph of the network is given in Figure 5.17

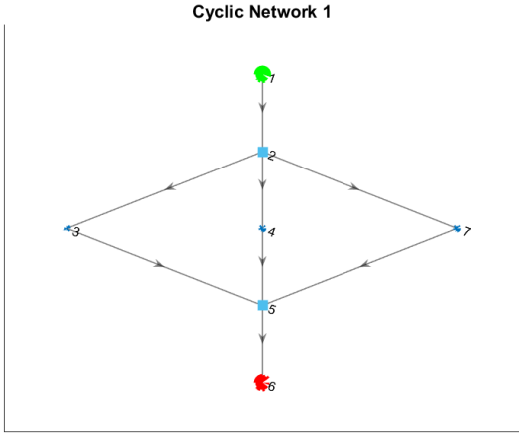

Figure 5.17: Simple Gas Cyclic Network

There is one source node, one demand node and two junction nodes. Our concern is to check the pressure and mass flow on supply and demand nodes. For now, we consider the case of same length and area of each pipe. The input data of the model is shown in Table 5.6.

Table 5.6: Given Data of Simple Cyclic Network

Description	Symbol	Value
Pressure at supply node	p_{s1}	30 bar
Flow rate at demand node	q_{d1}	30 kg/s
Area of each pipe	a	0.7854 m^2
Gamma	γ	1.46745319
Compressibility Factor	c	1
Mesh size	h	20
Length of each pipe	L	1000 m

We choose the $t = 1000$ *seconds* simulation time considering the above input parameters for the simulation of the network in the 5.17. The frequency response data has been

chosen for given interpolation points within random range. These interpolation points are used to construct ROM. To simulate the models, we keep the initial condition as zero. The results obtained from original and ROM have been plotted. Figure 5.18a and 5.18b show the mass flow at demand and supply node.

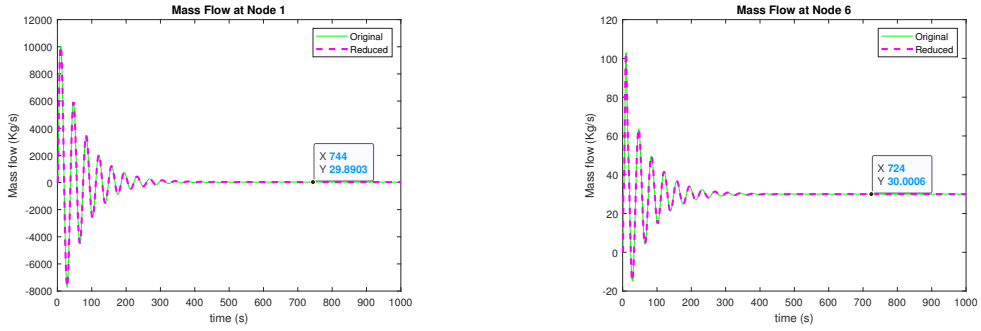

(a) Mass Flow at Supply Node **(b)** Mass Flow at Demand Node

Figure 5.18: Cyclic Network 1 Mass Flow

Similarly, we plot the pressure of the gas as well in Figure 5.19a and 5.19b

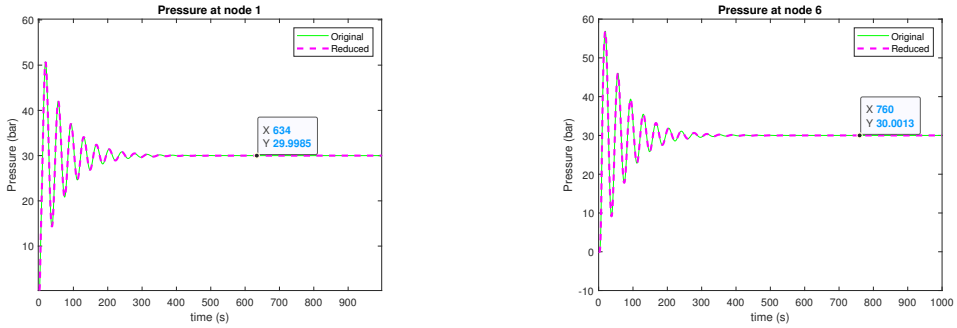

(a) Pressure at Supply Node **(b)** Pressure at Demand Node

Figure 5.19: Cyclic Network 1 Pressure

The comparison of results from original model and ROM can be observed from the error between both the results. The relative error is shown in Figure 5.20

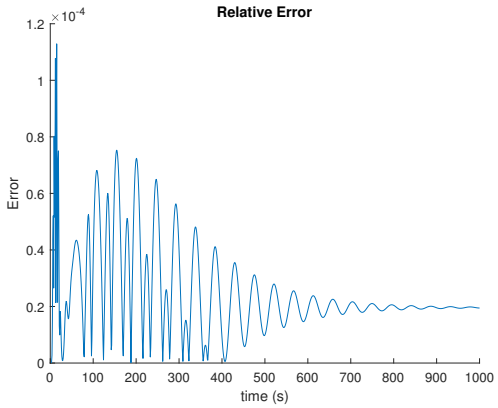

Figure 5.20: Cyclic Network 1 Relative Error

It is seen clearly that the ROM generates output with good accuracy while preserving the stability of original model. The size of the original model is $n = 504$ while the size of the reduced model is $r = 12$. The simulation time taken by ROM is 0.4511 *seconds* as compared to that of original model which is 6.6116 *seconds*. The ROM simulates easily and quickly with less computational power. Therefore, we can use the ROM for larger networks as well to make simulation faster.

5.5.2 Cyclic Network with Variable Parameters

We consider same cyclic network in Figure 5.4 but with different length, diameter and cross sectional area of each pipe. We consider the input of the model defined in Table 5.7

Table 5.7: Given Data of Variable Cyclic Network

Description	Symbol	Value
Pressure at supply node	p_{s1}	30 bar
Flow rate at demand node	q_{d1}	20 kg/s
Gamma	γ	1.46745319
Compressibility Factor	c	1
Mesh size	h	10

Next, we take length and area of each pipe as shown in Table 5.8

Table 5.8: Length and Cross-Sectional Area of Variable Cyclic Network

Pipe	**Length** (m)	**Area** (m^2)
Pipe12	2500	0.785
Pipe23	1600	0.685
Pipe24	1300	0.451
Pipe27	600	0.343
Pipe35	800	0.543
Pipe45	750	0.445
Pipe56	2100	0.331
Pipe75	500	0.423

We choose simulation time $t = 1000$ *seconds* for the above input parameters. The frequency response data has been chosen for given interpolation points . These interpolation points are used to build ROM. Define initial conditions as zero for simulation of the original and ROM. Figure 5.21a and 5.21b show the mass flow at demand and supply node.

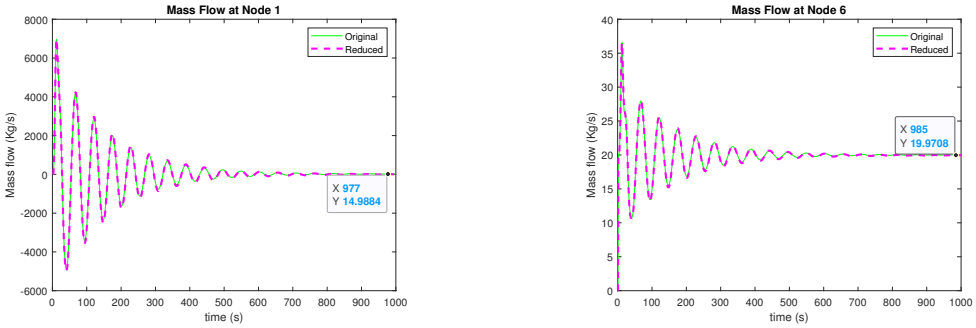

(a) Mass Flow at Supply Node

(b) Mass Flow at Demand Node

Figure 5.21: Cyclic Network 2 Mass Flow

Next, we look into pressure of the network at input and output node generated from both, original and reduced model. The pressure with respect to time can be seen in Figure 5.22a and 5.22b

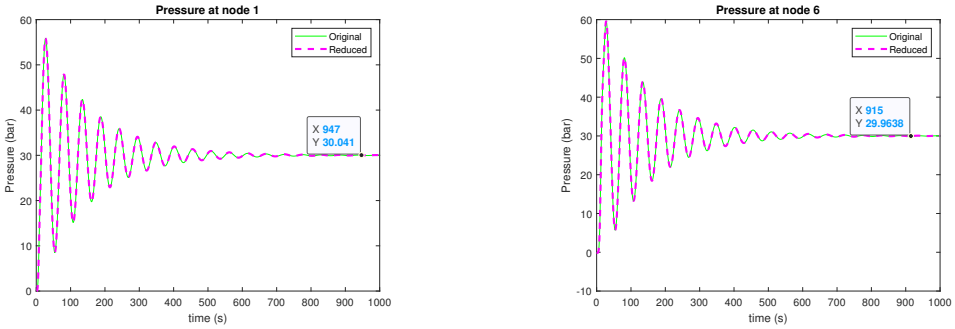

(a) Pressure at Supply Node

(b) Pressure at Demand Node

Figure 5.22: Cyclic Network 2 Pressure

The relative error in the results of reduced order model can be seen in Figure 5.23

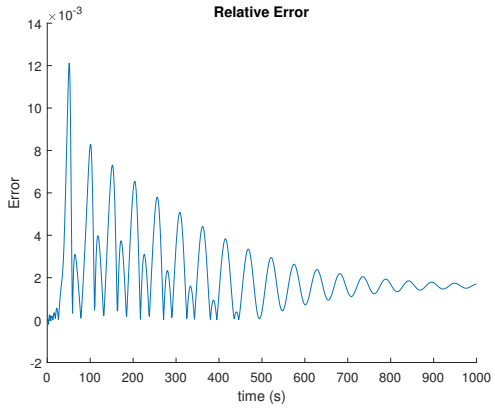

Figure 5.23: Cyclic Network 2 Relative Error

It is noted that the ROM generates output closely matching that of original model while reduced model is stable as well. The size of the full order model is $n = 1394$ while the size of the reduced mode constructed from l is $r = 12$. The total time taken by full order model to simulate is 106.47 *seconds* while the time taken to simulate the reduced model is 11.61 *seconds*. The ROM simulates easily and quickly with less computational power. Therefore, ROM can be used in modelling of large networks.

5.6 Large Network

In this section , we consider an example of modified part of gas distribution network. The graph of the network is shown in Figure 5.24.

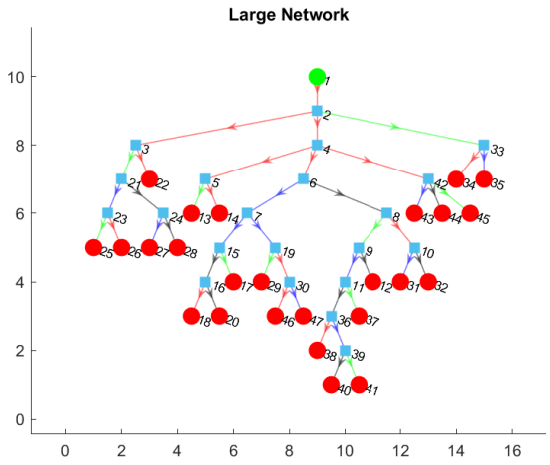

Figure 5.24: Large Gas Network

We consider input parameters of the original model as shown in Table 5.9

Table 5.9: Given Data of Large Network

Description	Symbol	Value
Pressure at supply node	p_{s1}	30 bar
Flow rate at each demand node	q_d	30 kg/s
Gamma	γ	1.46745319
Compressibility Factor	c	1
Mesh size	h	200
Length of each pipe	L	1000 m
Cross sectional area of each pipe	A	0.785 m^2

We choose simulation time $t = 8000$ *seconds* for the above input parameters. These interpolation points chosen randomly but all are unique; are used to construct ROM. The initial conditions for simulation of both, original and reduced model have been chosen as zero for the sake of simplicity. The mass flow and pressure at node 1 which is supply node are shown in Figure 5.25a and Figure 5.25b, respectively.

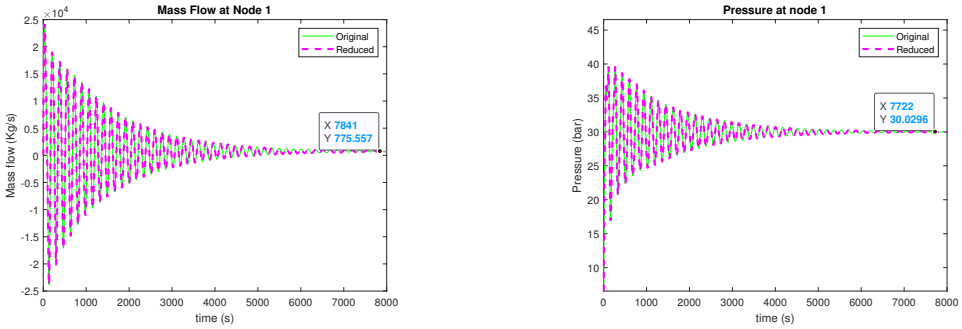

(a) Mass Flow at Supply Node **(b)** Pressure at Supply Node

Figure 5.25: Large Network Supply Node

Next, we check the pressure and mass flow at different demand nodes to see the graph converges at required mass flow and pressure in the steady state. The mass flow and pressure at node 37 can be seen in Figure 5.26a and Figure 5.26b, respectively.

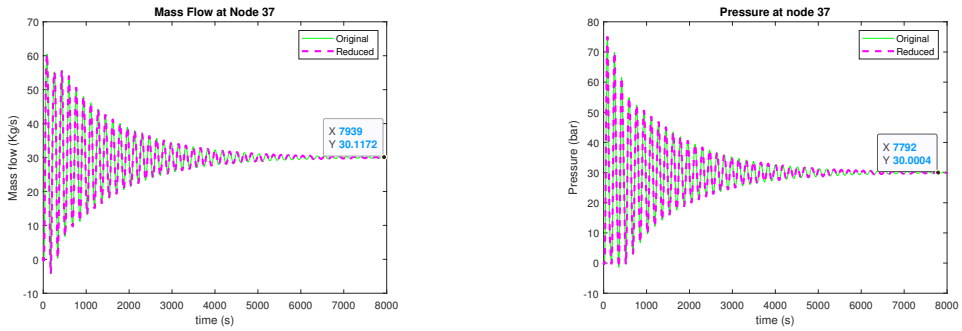

(a) Mass Flow at Demand Node **(b)** Pressure at Demand Node

Figure 5.26: Large Network Demand Node 27

Similarly, we checked the results at one more demand node to verify that original model as well as ROM generate stable responses. For node 41, the mass flow and pressure are shown in Figure 5.27a and 5.27b, respectively.

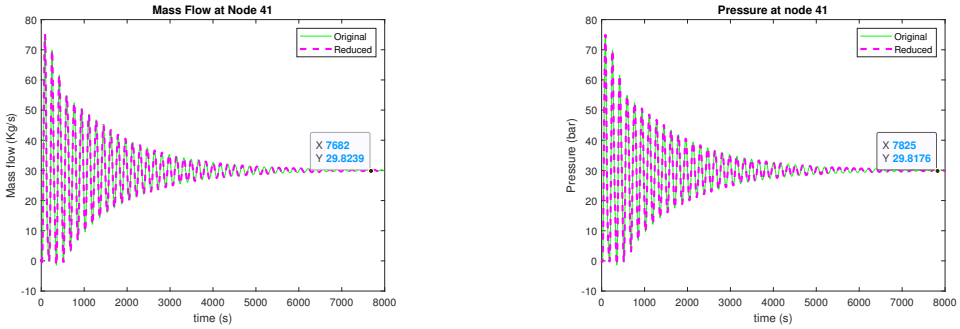

(a) Mass Flow at Demand Node

(b) Pressure at Demand Node

Figure 5.27: Large Network Demand Node 41

The absolute error between the results of FOM and ROM can be seen in Figure 5.28

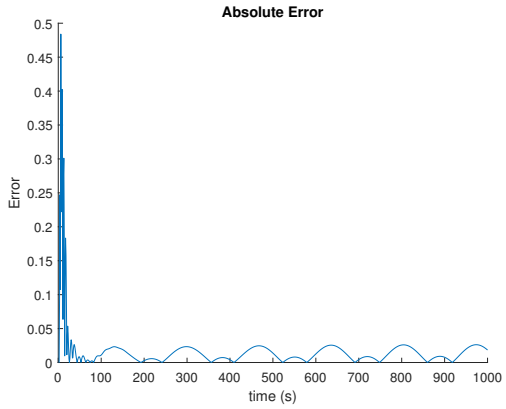

Figure 5.28: Large Network Absolute Error

It has been found that the ROM produces stable output results closely matching that of original model. The size of the full order model is $n = 481$ while the size of the reduced model constructed from data sets is $r = 140$. Further reduction of the model may produce unstable response. The issue can be resolved by using different set of tangential directions. Original model took 22.5913 *seconds* to simulate while the ROM took 3.1374 *seconds*. The accuracy of the ROM can be increases by many ways, one of which is to increase the size of reduction. Consequently, the simulation time for ROM will increase.

Chapter 6

Conclusion

6.1 Conclusion

In this thesis, the proposed methodology of choosing interpolation points for construction of ROM of the first- and second-order transfer functions of quadratic-bilinear systems has been tested for three different models. The results have also been compared with ROMs of the same size constructed using the interpolation points chosen by linear IRKA. In each case, the ROMs constructed using interpolation points from the greedy framework yield better approximation of the output than the ROMs constructed from IRKA. We then also develop a data driven model order reduction approach for simulation of gas distribution network modelled using 1D isothermal Euler equations. Firstly, different schemes of gas distribution network were designed. In the next phase, frequency response data of each network were collected at certain interpolation points. Using these datasets, we constructed ROM by applying Loewner framework. In this framework, a raw model was created at first and were then projected to subspace using SVD. We pointed out that the ROM constructed using Loewner framework created good approximation of original system while preserving the stability of the system at each output. It was also noted that the accuracy of ROM was based on choice of interpolation points as well as the tangential directions. We also noted that the ROM produced results faster than that of original model, yet generating the promising results with high accuracy. We noted that the Loewner framework provided trade-off between the accuracy of fit and size of the ROM. We also noted that the ROM generated using data driven approach was not structure dependent; hence proved to be better than POD in case of variable

input.

6.2 Future Work

The current approach of MOR was applied only to the linear version of the model in which the nonlinearity due to frictional factor and gravitational term were ignored. Apart from this, the interpolation points and tangential directions used in Loewner pencil matrix were chosen at random. The next phase of the research is to extend the given approach to nonlinear model of the gas network and define a mechanism to choose the optimal choice of interpolation points and tangential directions for linear as well as nonlinear model of gas network.

References

[1] A. Raza, R. Gholami, G. Meiyu, V. Rasouli, A. A. Bhatti, R. Rezaee, A review on the natural gas potential of pakistan for the transition to a low-carbon future, Energy Sources, Part A: Recovery, Utilization, and Environmental Effects 41 (9) (2019) 1149–1159.

[2] Y. Xie, X. Wang, F. Mai, Calculation of theoretical transmission loss in trunk gas pipeline, Advances in Mechanical Engineering 11 (12) (2019) 1687814019895440.

[3] A. C. Antoulas, Approximation of Large-Scale Dynamical Systems, Vol. 6 of Adv. Des. Control, SIAM Publications, Philadelphia, PA, 2005. doi:10.1137/1.9780898718713.

[4] R. W. Freund, The SPRIM algorithm for structure-preserving order reduction of general RCL circuits, in: Model Reduction for Circuit Simulation, Springer, 2011, pp. 25–52.

[5] W. Liu, H. Torsten, J. Drobnik, Effective thermal simulation of power electronics in hybrid and electric vehicles, World Electric Vehicle Journal 5 (2) (2012) 574–580.

[6] L. Feng, D. Koziol, E. B. Rudnyi, J. G. Korvink, Model order reduction for scanning electrochemical microscope: the treatment of nonzero initial condition, in: SENSORS, 2004 IEEE, IEEE, 2004, pp. 1236–1239.

[7] L. Feng, D. Koziol, E. Rudnyi, J. Korvink, Parametric model order reduction for scanning electrochemical microscopy: fast simulation of cyclic voltammogram, in: EuroSimE 2005. Proceedings of the 6th International Conference on Thermal, Mechanial and Multi-Physics Simulation and Experiments in Micro-Electronics and Micro-Systems, 2005., IEEE, 2005, pp. 55–59.

[8] E. B. Rudnyi, J. Lienemann, A. Greiner, J. G. Korvink, mor4ansys: Generating compact models directly from ansys models, in: Technical Proceedings of the 2004 Nanotechnology Conference and Trade Show, Nanotech, Vol. 2, 2004, pp. 279–282.

[9] S. O. Han, K. Wolf, H. Hanselka, T. Bein, Design and analysis of an adaptive vibration isolation system considering large scale parameter variations, in: Active and Passive Smart Structures and Integrated Systems 2009, Vol. 7288, International Society for Optics and Photonics, 2009, p. 728829.

[10] A. C. Antoulas, D. C. Sorensen, Approximation of large-scale dynamical systems: An overview, Int. J. Appl. Math. Comput. Sci. 11 (5) (2001) 1093–1121.

[11] B. Moore, Principal component analysis in linear systems: Controllability, observability, and model reduction, IEEE Transactions on Automatic Control 26 (1) (1981) 17–32. doi:10.1109/TAC.1981.1102568.

[12] V. Mehrmann, T. Stykel, Balanced truncation model reduction for large-scale systems in descriptor form, in: Dimension Reduction of Large-Scale Systems, Springer, 2005, pp. 83–115.

[13] E. I. Verriest, Time Variant Balancing and Nonlinear Balanced Realizations, Springer Berlin Heidelberg, Berlin, Heidelberg, 2008, pp. 213–250. doi:10.1007/978-3-540-78841-6_11.
URL https://doi.org/10.1007/978-3-540-78841-6_11

[14] M. S. Tombs, I. Postlethwaite, Truncated balanced realization of a stable non-minimal state-space system, International Journal of Control 46 (4) (1987) 1319–1330.

[15] W. H. Schilders, H. A. Van der Vorst, J. Rommes, Model order reduction: theory, research aspects and applications, Vol. 13, Springer, 2008.

[16] A. Vandendorpe, P. Van Dooren, Model reduction of interconnected systems, in: W. H. A. Schilders, H. A. van der Vorst, J. Rommes (Eds.), Model Order Reduction: Theory, Research Aspects and Applications, Vol. 13 of Mathematics in Industry, Springer, Berlin, Heidelberg, 2008, pp. 305–321. doi:10.1007/978-3-540-78841-6_14.

[17] C. A. Beattie, S. Gugercin, Model reduction by rational interpolation, Model Reduction and Algorithms: Theory and Applications, P. Benner, A. Cohen, M. Ohlberger, and K. Willcox, eds., Comput. Sci. Engrg 15 (2017) 297–334.

[18] U. Baur, P. Benner, L. Feng, Model order reduction for linear and nonlinear systems: A system-theoretic perspective, Arch. Comput. Methods Eng. 21 (4) (2014) 331–358. doi:10.1007/s11831-014-9111-2.

[19] E. J. Grimme, Krylov projection methods for model reduction, Ph.D. Thesis, Univ. of Illinois at Urbana-Champaign, USA (1997).
URL https://perso.uclouvain.be/paul.vandooren/ThesisGrimme.pdf

[20] A. C. Antoulas, D. C. Sorensen, S. Gugercin, A survey of model reduction methods for large-scale systems, Contemp. Math. 280 (2001) 193–219.

[21] C. Gu, QLMOR: A projection-based nonlinear model order reduction approach using quadratic-linear representation of nonlinear systems, IEEE Trans. Comput. Aided Des. Integr. Circuits. Syst. 30 (9) (2011) 1307–1320. doi:10.1109/TCAD.2011.2142184.

[22] P. Benner, T. Breiten, Two-sided projection methods for nonlinear model order reduction, SIAM J. Sci. Comput. 37 (2) (2015) B239–B260. doi:10.1137/14097255X.

[23] M. I. Ahmad, P. Benner, I. Jaimoukha, Krylov subspace projection methods for model reduction of quadratic-bilinear systems, IET Control Theory & Applications 10 (16) (2016) 2010–2018. doi:10.1049/iet-cta.2016.0415.

[24] R. J. Rugh, Nonlinear System Theory, Johns Hopkins University Press Baltimore, MD, 1981.

[25] P. Benner, P. Goyal, S. Gugercin, $\mathcal{H}_2$-quasi-optimal model order reduction for quadratic-bilinear control systems, arXiv preprint arXiv:1610.03279 (2016).

[26] A. J. Mayo, A. C. Antoulas, A framework for the solution of the generalized realization problem, Linear Algebra Appl. 425 (2-3) (2007) 634–662, special Issue in honor of P. A. Fuhrmann, Edited by A. C. Antoulas, U. Helmke, J. Rosenthal, V. Vinnikov, and E. Zerz.

[27] A. C. Ionita, A. C. Antoulas, Data-driven parametrized model reduction in the Loewner framework, SIAM J. Sci. Comput. 36 (3) (2014) A984–A1007. doi:10.1137/130914619.

[28] I. V. Gosea, A. C. Antoulas, Model reduction of linear and nonlinear systems in the Loewner framework: A summary„ in: 14th European Control Conference (ECC), July 15–17, Linz, Austria, 2015, pp. 345–349. doi:10.1109/ECC.2015.7330568.

[29] M. Ahmad, L. Feng, P. Benner, A new interpolatory model reduction for quadratic bilinear descriptor systems, Proc. Appl. Math. Mech. 15 (1) (2015) 589 – 590.

[30] M. I. Ahmad, P. Benner, L. Feng, Interpolatory model reduction for quadratic-bilinear systems using error estimators, Engineering Computations (2018).

[31] S. Grundel, N. Hornung, B. Klaassen, P. Benner, T. Clees, Computing Surrogates for Gas Network Simulation using Model Order Reduction, Springer New York, 2013, pp. 189–212. doi:10.1007/978-1-4614-7551-4_9.

[32] K. Kunisch, S. Volkwein, Proper orthogonal decomposition for optimality systems, ESAIM: Math. Model. Numer. Anal. 42 (1) (2008) 1–23.

[33] J. R. Phillips, Projection-based approaches for model reduction of weakly nonlinear, time-varying systems, IEEE Trans. Comput.-Aided Design Integr. Circuits Syst. 22 (2) (2003) 171–187.

[34] M. A. Khattak, M. I. Ahmad, L. Feng, P. Benner, Multivariate moment matching for model order reduction of quadratic-bilinear systems using error bounds, arXiv preprint arXiv:2105.12966 (2021).

[35] L. Feng, A. C. Antoulas, P. Benner, Some a posteriori error bounds for reduced order modelling of (non-)parametrized linear systems, Preprint MPIMD/15-17, Max Planck Institute Magdeburg, available from http://www.mpi-magdeburg.mpg.de/preprints/ (Oct. 2015).

[36] T. G. Kolda, B. W. Bader, Tensor decompositions and applications, SIAM Rev. 51 (3) (2009) 455–475.

[37] Y. Hongdong, Y. Yun, Steady-state model and its application in natural gas during transportation in pipeline, in: 2012 Fourth International Conference on Computational and Information Sciences, IEEE, 2012, pp. 1248–1250.

[38] M. Abeysekera, J. Wu, N. Jenkins, M. Rees, Steady state analysis of gas networks with distributed injection of alternative gas, Applied Energy 164 (2016) 991–1002.

[39] A. Bermúdez, J. González-Díaz, F. J. González-Diéguez, Á. M. González-Rueda, M. P. F. de Córdoba, Simulation and optimization models of steady-state gas transmission networks, Energy Procedia 64 (2015) 130–139.

[40] A. Ekhtiari, I. Dassios, M. Liu, E. Syron, A novel approach to model a gas network, Applied Sciences 9 (6) (2019) 1047.

[41] A. Osiadacz, Simulation of transient gas flows in networks, International journal for numerical methods in fluids 4 (1) (1984) 13–24.

[42] Chapter 11 - sales gas transmission, in: S. Mokhatab, W. A. Poe, J. G. Speight (Eds.), Handbook of Natural Gas Transmission and Processing, Gulf Professional Publishing, Burlington, 2006, pp. 401–430. doi:https://doi.org/10.1016/B978-075067776-9/50016-6.
URL https://www.sciencedirect.com/science/article/pii/B9780750677769500166

[43] A. Herrán-González, J. De La Cruz, B. De Andrés-Toro, J. L. Risco-Martín, Modeling and simulation of a gas distribution pipeline network, Applied Mathematical Modelling 33 (3) (2009) 1584–1600.

[44] J. Szoplik, The gas transportation in a pipeline network, Advances in Natural Gas Technology (2012).

[45] P. Wang, S. Ao, B. Yu, D. Han, Y. Xiang, An efficiently decoupled implicit method for complex natural gas pipeline network simulation, Energies 12 (8) (2019) 1516.

[46] R. Madoliat, E. Khanmirza, H. R. Moetamedzadeh, Transient simulation of gas pipeline networks using intelligent methods, Journal of Natural Gas Science and Engineering 29 (2016) 517–529.

[47] M. Gugat, M. Herty, Modeling, control and numerics of gas networks, arXiv preprint arXiv:2010.02743 (2020).

[48] A. D. Woldeyohannes, M. A. Abd Majid, Simulation model for natural gas transmission pipeline network system, Simulation Modelling Practice and Theory 19 (1) (2011) 196–212.

[49] R. Gupta, T. Prasad, Extended use of linear graph theory for analysis of pipe networks, Journal of hydraulic engineering 126 (1) (2000) 56–62.

[50] M. Gugat, G. Leugering, F. Hante, Stationary states in gas networks (2016).

[51] R. Z. Ríos-Mercado, C. Borraz-Sánchez, Optimization problems in natural gas transportation systems: A state-of-the-art review, Applied Energy 147 (2015) 536–555.

[52] H. S. Lall, P. B. Percell, A dynamic programming based gas pipeline optimizer, in: Analysis and Optimization of Systes, Springer, 1990, pp. 123–132.

[53] H. Shuai, X. Ai, J. Fang, T. Ding, Z. Chen, J. Wen, Real-time optimization of the integrated gas and power systems using hybrid approximate dynamic programming, International Journal of Electrical Power & Energy Systems 118 (2020) 105776.

[54] M. HACIBEYOĞLU, M. H. IBRAHIM, Comparison of the effect of unsupervised and supervised discretization methods on classification process, International Journal of Intelligent Systems and Applications in Engineering (2016) 105–108.

[55] S. Chen, L. Tang, W. Liu, Y. Li, A improved method of discretization of continuous attributes, Procedia Environmental Sciences 11 (2011) 213–217.

[56] C. H. Brito, C. B. Maia, J. R. Sodre, A mathematical model for the exhaust gas temperature profile of a diesel engine, in: Journal of Physics: Conference Series, Vol. 633, IOP Publishing, 2015, p. 012075.

[57] P. Wang, B. Yu, D. Han, J. Li, D. Sun, Y. Xiang, L. Wang, Adaptive implicit finite difference method for natural gas pipeline transient flow, Oil & Gas Sciences and Technology–Revue d'IFP Energies nouvelles 73 (2018) 21.

[58] J. F. Helgaker, B. Müller, T. Ytrehus, Transient flow in natural gas pipelines using implicit finite difference schemes, Journal of Offshore Mechanics and Arctic Engineering 136 (3) (2014).

[59] C. O. Malley, D. Kourounis, G. Hug, O. Schenk, Finite volume methods for transient modeling of gas pipelines, in: 2018 IEEE International Energy Conference (ENERGYCON), IEEE, 2018, pp. 1–6.

[60] W. Hai, L. Xiaojing, Z. Weiguo, Transient flow simulation of municipal gas pipelines and networks using semi implicit finite volume method, Procedia Engineering 12 (2011) 217–223.

[61] Y. Qiu, S. Grundel, M. Stoll, P. Benner, Efficient numerical methods for gas network modeling and simulation, arXiv preprint arXiv:1807.07142 (2018).

[62] M. Herty, J. Mohring, V. Sachers, A new model for gas flow in pipe networks, Mathematical Methods in the Applied Sciences 33 (7) (2010) 845–855.

[63] S. Grundel, N. Hornung, B. Klaassen, P. Benner, T. Clees, Computing surrogates for gas network simulation using model order reduction, in: Surrogate-Based Modeling and Optimization, Springer, 2013, pp. 189–212.

[64] V. Gyrya, A. Zlotnik, An explicit staggered-grid method for numerical simulation of large-scale natural gas pipeline networks, Applied Mathematical Modelling 65 (2019) 34–51.

[65] S. Ke, H. Ti, Transient analysis of isothermal gas flow in pipeline network, Chemical Engineering Journal 76 (2) (2000) 169–177.

[66] T. Clees, Parameter studies for energy networks with examples from gas transport, in: Simulation-Driven Modeling and Optimization, Springer, 2016, pp. 29–54.

[67] M. K. Banda, M. Herty, A. Klar, Coupling conditions for gas networks governed by the isothermal euler equations, Networks & Heterogeneous Media 1 (2) (2006) 295.

[68] P. Benner, S. Grundel, C. Himpe, C. Huck, T. Streubel, C. Tischendorf, Gas network benchmark models, in: Applications of Differential-Algebraic Equations: Examples and Benchmarks, Springer, 2018, pp. 171–197.

[69] A. Antoulas, A. Ionita, S. Lefteriu, On two-variable rational interpolation, Linear Algebra and its Applications 436 (8) (2012) 2889–2915.

[70] I. V. Gosea, Model order reduction of linear and nonlinear systems in the loewner framework, Ph.D. thesis, PhD thesis, Department of Electrical Engineering, Jacobs University, Bremen ... (2017).

[71] Y. Chen, Model reduction for nonlinear systems, Master's thesis, Massachusetts Institute of Technology (1999).

Appendices

.1 Greedy Framework Algorithm

Algorithm 1 An adaptive framework for selection of interpolation points

Inputs: σ_{10}, σ_{20}, E, A, N, H, B, C and S_{sample}: a set of the samples of $\mu := (s_1, s_2)$, which covers the domain of the two frequency variables.

Outputs: μ, V and W

Initialization: $V = [\ ]$; $W = [\ ]$; $V_1 = [\ ]$; $W_1 = [\ ]$; $V_2 = [\ ]$; $W_2 = [\ ]$; $\epsilon = 1$; $i = -1$; $j = 0$; $\epsilon_{tol} < 1$, $\mu^0 = (\sigma_{10}, \sigma_{20})$.

WHILE $\epsilon > \epsilon_{tol}$

1 $i = i + 1$; $j = j + 1$;

2 compute $\bar{V}_i(\sigma_{1i})$ and $\bar{W}_i(\sigma_{1i})$ using (3.3.3)

3 $V_1 = orth[V_1, \bar{V}_i]$; $W_1 = orth[W_1, \bar{W}_i]$;

4 $\sigma_{1j} = \arg \max_{\sigma_1 \in S_{1\ \text{sample}}} \Delta_1(\sigma_1)$;

5 compute $V_i(\sigma_{1i}, \sigma_{2i})$ and $W_i(\sigma_{1i}, \sigma_{2i})$ using (3.3.8)

6 $V_2 = orth[V_2, V_i]$; $W_2 = orth[W_2, W_i]$;

7 $\sigma_{2j} = \arg \max_{\sigma_2 \in S_{2\ \text{sample}}} \Delta_2(\sigma_{1i}, \sigma_2)$;

8 $\mu^j = [\sigma_{1j}, \sigma_{2j}]$;

9 $V = orth[V_1, V_2]$; $W = orth[W_1, W_2]$;

10 $\Delta(\mu^j) := \Delta_1(\mu^j) + \Delta_2(\mu^j)$; $\epsilon = \Delta(\mu^j)$;

END WHILE.